Simulation Study of the Determination of Temperature of QGP produced in the CBM experiment using Thermal Dileptons

M.Sc. Thesis

by

PRASOON CHAKRABORTY

Roll No:-1703151014

Thesis Supervisor : Dr. Ankhi Roy

PSPC members : Dr.Manavendra Mahato

:Dr. Anand Parkash

June 2019

Discipline of Physics

INDIAN INSTITUTE OF TECHNOLOGY INDORE

Khandwa Road, simrol-452020

Simulation Study of the Determination of Temperature of QGP produced in the CBM experiment using Thermal Dileptons

A thesis

Submitted in partial fulfillment of the requirements for the award of the degree of

Master of Science

by

Prasoon Chakraborty

Discipline of Physics

Indian Institute of Technology Indore

Khandwa Road, Simrol-452020

June 2019

I hereby certify that the work which is being presented in the thesis entitled **Simulation Study of the Determination of Temperature of QGP produced in the CBM experiment using Thermal Dileptons** in the partial fulfillment of the requirements for the award of the degree of **MASTER OF SCIENCE** and submitted in the **DISCIPLINE OF PHYSICS, INDIAN INSTITUTE OF TECHNOLOGY INDORE**, is an authentic record of my own work carried out during the time period from July, 2018 to June, 2019 under the supervision of **Dr. Ankhi Roy**, Associate Professor, Discipline of Physics, IIT Indore.

The matter presented in this thesis has not been submitted by me for the award of any other degree of this or any other institute.

Signature of the student with date
(PRASOON CHAKRABORTY)

This is to certify that the above statement made by the candidate is correct to the best of my knowledge.

Sign. of Thesis Supervisor with date
(Dr. Ankhi Roy)

PRASOON CHAKRABORTY has successfully given his M.Sc. Oral Examination held on 21 June, 2019.

Signature of Thesis Supervisor	Convener, DPGC
Date:	Date:
Sign. of PSPC Member #1	Sign. of PSPC Member #2
Dr.Manavendra Mahato	Dr.Anand Parkash
Date:	Date:

I do not know what I may appear to the world; but to myself, I seem to have been only like a boy playing on the seashore, and diverting myself now and then in finding a smoother pebble or prettier shell than ordinary, while the great ocean of truth lay all undiscovered before me.

-Sir Isaac Newton

5

Acknowledgement

First and foremost, I would pay my sincere gratitude and thanks to my research supervisor Dr.Ankhi Roy for her guidence, immense knowledge, continuous support and encouragement throughout my research. For her constant motivation and stimulating discussions related to my research which has benefitted me immensely. For being patient with me at times when I have struggled. I am thankful.

I would also like to express my sincere respect and gratitude to my PSPC members Dr. Manavendra Mahato and Dr. Anand Parkash for their crucial and thoughtful comments and constant encouragement, and also for their critical questions and queries which has allowed me to ponder over my research from different perspectives.

I am immensely indebted to Prof.Partha Pratim Bhaduri of Variable Energy Cyclotron Centre(VECC), Kolkata, for his extremely crucial remarks and guidence related to my work. For his expert comments and suggestions while I was doing Summer Student Program at VECC. I am thankful.

I am extremely thankful to Mr.Sumit Kundu, Mr.Sudhir Pandurang rode and Mr. Ravindra singh for there encouragement and crucial support. I am also thankful to all my classmates who have helped me throughout my academic journey here at IIT Indore.

Last but not the least, I would like to thank my parents who have made it possible for me to persue my dreams and aspirations and who have guided me in all aspects of my life. I am fortunate to have been a recipient of the academic environment provided here at IIT Indore which has inspired me immensely.

Prasoon Chakraborty
M.Sc., Final year
Discipline of Physics
IIT Indore

Abstract

Nuclear matter is expected to exist in various phases and it's phase transitions are mapped on a phase diagram that has been created using Quantum Chromodynamics which is the leading theory governing the interaction of quarks and gluons that make up the nuclear matter. One of the predicted phases of the nuclear matter is the quark gluon plasma in which the system evolves from a hadronic to partonic degrees of freedom. QGP is a hot thermal medium and Boltzmann statistics is reasonably applicable for all thermodynamic quantities. Hence, the invariant mass distribution of the thermally equilibrated matter will follow an exponential decay and the inverse of the slope of the exponential decay will provide the average temperature of the QGP. The most important condition that a possible probe must satisfy for the measurement of the temperature of the QGP is that they must have mean free path longer than the total size of the QGP medium. A large mean free path indicates a small interaction cross section as mean free path is inversely proportional to the interaction cross section. That means that hadrons are not good probes for measuring the temperature of QGP medium as they have significant interaction cross section as they interact through the strong force and hence their initial invariant mass distribution is modified before reaching any detector in heavy ion experiments. An ideal probe therefore should interact electromagnetically and not via strong force. Leptons and photons satisfy such criteria. Hence thermal dileptons produced from the annihilation of quark and antiquark in the QGP medium could be used to extract the temperature of the QGP.In this simulation work, we have taken 200k thermal Dimuons which is generated using the PLUTO event generator and analyzed various attributes of the Dimuon spectra. Next, We have analyzed the invariant mass distribution of

these thermal dimuons without passing them through any detector setup. The CBM experiment is a future project that is designed to probe nuclear matter at high baryon density. So, Next we have passed these 200k dimuons through the entire CBM detector simulation setup and obtained the invariant mass distribution at the MUCH detector of the CBM experiment. Next we have created the background particles in a heavy ion collision using UrQMD event generator and passed both signal dimuons and background particles through the entire CBM setup and obtained the invariant mass distribution. Next we have only used background from UrQMD and passed them through the CBM setup and obtained the invariant mass distribution of the background particles at the MUCH detector. And finally we have subtracted the background from the entire realistic event created using both PLUTO and UrQMD and obtained the subtracted invariant mass spectra at the MUCH detector to get an estimate of temperature measurement capabilities of the CBM experiment.

List of Figures

1.1 QCD Phase Diagram 20
1.2 Schematic diagram showing the space time evolution of different stages of the heavy ion collisions 20

2.1 Details of the CBM Experiment 32
2.2 Schematic view of the MUCH SIS100-B configuration. It consists of 12 detector layers and 4 absorbers including the first absorber of 60cm carbon 34
2.3 Schematic view of the layout of the muon chambers with trapezoidal overlapping sectors 35
2.4 Details Of the trapezoidal section of a detector layer with PCB . 36

3.1 P and Pt distribution comparison at station 1 layer 3 for primary particles 38
3.2 P and Pt distribution comparison at station 1 layer 3 for secondary particles 39
3.3 P and Pt distribution at station 2 layer 3 for primary particles . 39
3.4 P and pt distribution at station 2 layer 3 for secondary particles 40
3.5 P and Pt distribution of primary particles for the entire MUCH system 40
3.6 P and pt distribution for secondary particles for the entire MUCH system 41
3.7 P and pt distribution for all particles at station 1 layer 3 of the MUCH Detector. 41
3.8 P and pt distribution for all particles at station 2 layer 3 of the MUCH Detector. 42

3.9 P and pt distribution for all particles for the entire MUCH Detector. . . . 42
3.10 P and pt distribution for primary pion particles for the entire MUCH Detector. . . . 43
3.11 P and pt distribution for primary proton particles for the entire MUCH Detector. . . . 43
3.12 P and pt distribution for secondary pion particles for the entire MUCH Detector. . . . 44
3.13 P and pt distribution for secondary proton particles for the entire MUCH Detector. . . . 44

4.1 Momentum distribution of dimuons obtained using PLUTO . . 49
4.2 The energy distribution of dimuons 50
4.3 Transverse momentum distribution of dimuons obtained from PLUTO 50
4.4 The rapidity distribution of dimuons 51
4.5 The pseudorapidity distribution of dimuons 51
4.6 The variation of the cosine of the opening angle between two muons in the dimuon 52
4.7 The variation of the opening angle between two muons in a dimuon measured in radians 53
4.8 The variation of the opening angle with respect to energy 53
4.9 invariant mass distribution of signal dimuons 54
4.10 The energy distribution for each muon 55
4.11 The momentum distribution for each muon 56
4.12 The transverse momentum distribution for each muon 56
4.13 The rapidity distribution for each muon 57
4.14 The pseudorapidity distribution for each muon 57
4.15 The invariant mass distribution for each muon 58
4.16 The energy distribution of reconstructed dimuons. 59
4.17 The momentum distribution of reconstructed dimuons. 59
4.18 The transverse momentum distribution of reconstructed dimuons. 60
4.19 The rapidity distribution of reconstructed dimuons. 60

4.20 The pseudorapidity distribution of reconstructed dimuons. . . . 61
4.21 The distribution of cosine of the opening angle of reconstructed dimuon pair 61
4.22 The distribution of the opening angle of reconstructed dimuon pair 62
4.23 The distribution of the opening angle with respect to energy for reconstructed dimuon pair 62
4.24 Invariant mass distribution of reconstructed thermal dimuons for complete range of transverse momentum. 63
4.25 Invariant mass distribution of reconstructed thermal dimuons having transverse momentum between 0.0 GeV/C to 0.5 GeV/C 64
4.26 Invariant mass distribution of reconstructed thermal dimuons having transverse momentum between 0.5 GeV/C to 1 GeV/C . 65
4.27 Invariant mass distribution of reconstructed thermal dimuons having transverse momentum between 1 GeV/C to 1.5 GeV/C . 66
4.28 Invariant mass distribution of the reconstructed background for the entire p_t range. 68
4.29 Invariant mass distribution of the reconstructed background for the p_t range from 0.0 GeV/C to 0.5 GeV/C. 68
4.30 Invariant mass distribution of the reconstructed background for the p_t range from 0.5 GeV/C to 1 GeV/C. 69
4.31 Invariant mass distribution of the reconstructed background for the p_t range from 1 GeV/C to 1.5 GeV/C. 69
4.32 Invariant mass distribution of the reconstructed combined signal and background for the complete p_t range 70
4.33 Invariant mass distribution of the reconstructed combined signal and background for the p_t range from 0.0 GeV/C to 0.5 GeV/C. 71
4.34 Invariant mass distribution of the reconstructed combined signal and background for the p_t range from 0.5 GeV/C to 1 GeV/C. . 71
4.35 Invariant mass distribution of the reconstructed combined signal and background for the p_t range from 1 GeV/C to 1.5 GeV/C. . 72

4.36 Invariant mass distribution of the reconstructed signal obtained after subtracting the background from the entire combined signal and background for entire p_t range 73
4.37 Invariant mass distribution of the reconstructed signal obtained after subtracting the background from the entire combined signal and background for p_t range from 0.0 GeV/C to 0.5 GeV/C 74
4.38 Invariant mass distribution of the reconstructed signal obtained after subtracting the background from the entire combined signal and background for p_t range from 0.5 GeV/C to 1 GeV/C . 75

List of Tables

4.1 Tabulated summary of PLUTO analysis 66

4.2 Tabulated summary of analysis of signal obtained after background subtraction 75

4.3 Tabulated summary of analysis for pure PLUTO, Reconstructed PLUTO as well as for signal obtained after background subtraction. 76

Contents

1 Introduction **17**

1.0.1 1.1 Space-Time evolution of Heavy ion Collisions 20

1.0.2 1.2 Thermal Dileptons and the temperature of the QGP 22

2 The CBM Experiment **28**

2.0.1 2.1 Basic Science behind Muon Identification in CBM Experiment 28

2.0.2 2.2 Details of the CBM Experiment 30

2.0.3 2.2.1 Dipole magnet: 30

2.0.4 2.2.2 Micro-Vertex Detector (MVD): 30

2.0.5 2.2.3 Silicon Tracking System (STS): 30

2.0.6 2.2.4 Ring Imaging Cherenkov Detector (RICH): 31

2.0.7 2.2.5 Muon Chamber System (MUCH): 31

2.0.8 2.2.6 Transition Radiation Detector (TRD): 32

2.0.9 2.2.7 Timing Multi-gap Resistive Plate Chambers (MRPC): 32

2.0.10 2.2.8 Electromagnetic Calorimeter (ECAL): 33

2.0.11 2.2.9 Projectile Spectator Detector (PSD) 33

2.0.12 2.3 Details of the various components of the MUCH Detector 33

2.0.13 2.4 Details of the Detectors within the MUCH System . 34

3 ANALYSIS 1 **37**

3.0.1 3.1 Analysis of momentum and transverse momentum distrbution of primary and secondary particles 38

3.0.2 3.2 Conclusion 45

4 Analysis 2 **46**

4.0.1 4.1 Analysis of the signal thermal dimuons 48

4.0.2 4.3 Analysis of various kinematic variables of the signal dimuons after passing them through the CBM setup . . . 58

4.0.3 4.4 Analysis of the background particles 67

4.0.4 4.5 Analysis of the signal and background combined together 70

4.0.5 4.6 Analysis of the reconstructed signal after removing the background from complete spectra. 72

4.0.6 4.7 Conclusion and Future Scope of this Work. 76

Chapter 1

Introduction

We know that matter is made up of atoms. In our everyday surrounding,we observe various different states of matter ranging from solids to liquids and gases.However, through rigorous experimental and theoretical investigations into the nature of matter it has been established that,atoms have internal structures. They are further made of electrons and a nucleus which consists of hadrons namely protons and neutrons. These hadrons are further made of quarks which are confined within the hadrons through strong interactions mediated by gluons. In experimental high energy physics,the study of different phases of this nuclear matter inside atoms is one of the most highly investigated topic. These investigations lead us to a better understanding of how matter behaves and interacts in extreme environments with extreme temperatures and densities. Normal nuclei consists of protons and neutrons with their net baryon density normalized to one. Nucleons are excited to short-lived baryonic resonances at moderate temperature and densities , which decay by the emission of mesons.Additional baryon- antibaryon pairs are created,At higher temperatures.If baryons have a majority then this mixture of baryons,antibaryons and mesons,Which are all strongly interacting particles, is generally called hadronic matter,or baryonic matter. At very high temperatures or densities the hadrons melt,and the constituents, the quarks and gluons, form a new phase, the Quark-Gluon-Plasma .A quark gluon plasma is a state of matter in quantum chromodynamics (QCD) which exists at extremely high temperature and/or density. This state is thought to consist of asymptotically free strongly interacting quarks and gluons , which are ordinarily confined by color confinement inside atomic nuclei or other hadrons.In the Standard Model of particle physics the strong interaction is explained by a relativistic quantum field theory called Quantum Chromodynamics(QCD).The fundamental degrees of freedom in QCD are point-like particles called quarks and gluons. Quarks occur in six different flavors namely up, down, strange, charm, bottom, top.Quarks and gluons also carry an additional quantum number called color charge.The transition from hadronic phase to QGP phase is smooth at low baryon densities.QGP forms at a temperature of about 156 MeV. The QCD phase diagram has been created from the calculations based on quantum chromodynamics .The objective of high energy physics is basically to verify and establish the validity of this phase diagram. To achieve this we have to investigate the nuclear matter at different energy ranges and particle densities and hence,different particle accelerators have been constructed around the world that function at different energy ranges.QCD is however different from QED(quantum electrodynamics) in the sense that in QCD,the gauge bosons,that is,the gluons carry color charge,and hence interact with each other unlike in the case of QED where the photons do not interact with each other as they do not carry any electric charge whatsoever.This leads to variation of the QCD coupling constant due to self interaction of gluons. The coupling constant decreases logarithmically with increasing momentum transfer. Hence the coupling constant decreases with decrease in separation between the quarks.which leads to asymptotic freedom.Hence the strong force of attraction between quarks increases with increasing distance between them. This phenomenon is called infrared slavery leading to quark confinement.Hence no free quarks are observed in nature. At very low baryon density and at high temperature or vice versa, a highly dense environment of quarks and gluons is obtained,hence quarks and gluons can be considered as degrees of free- dom of this new state of matter. This new state of quark matter is called the quark-gluon plasma (QGP). QGP is a locally thermally equilibrated state of matter in which quarks and gluons are deconfined from hadrons, and color degrees of freedom become significant.The following diagram shows the Phase transition of strongly interacting matter as a function of the temperature T and the baryon-chemical potential μ_B. For very low net baryon densities the transition is expected to be smooth from hadronic matter to a hot mixture of quarks and gluons, above a temperature of about 156 MeV. In this part of the phase diagram beyond cer- tain critical point, one expects a first order phase transition from hadronic to partonic matter at larger values of net baryon densities.The QGP matter has been probed by colliding heavy ions at the Relativistic Heavy Ion Collider (RHIC) at Brookhaven National Laboratory, New York,USA and the Large Hadron Collider (LHC) at CERN, Geneva. The LHC creates QGP in the laboratory by creating a state of very high temperature and densities, whereas the CBM experiment at FAIR facility at GSI, Darmstadt ,Germany will create the same by producing high baryon density matter through high compression which is achieved by high energy nucleus-nucleus collision.This would allow the study of the equation-of-state of nuclear matter at core densities possible inside the neutron stars,and search for phase transitions, exotic forms of (strange) QCD matter and chiral symmetry restoration. The CBM detector is designed to measure the collective behavior of hadrons, together with detection and analysis of rare diagnostic probes such as multistrange hyperons, charmed particles and vector mesons decaying into lepton pairs with never before obtained precision and statistics.This will also therefore open new windows into the physics of exotic matter[1].

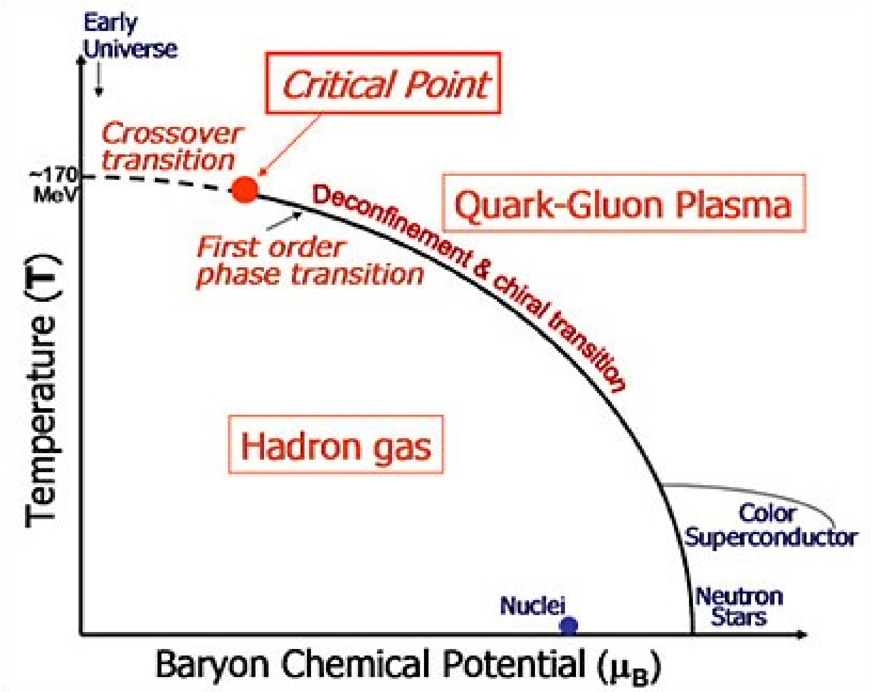

Figure 1.1: QCD Phase Diagram

1.1 Space-Time evolution of Heavy ion Collisions

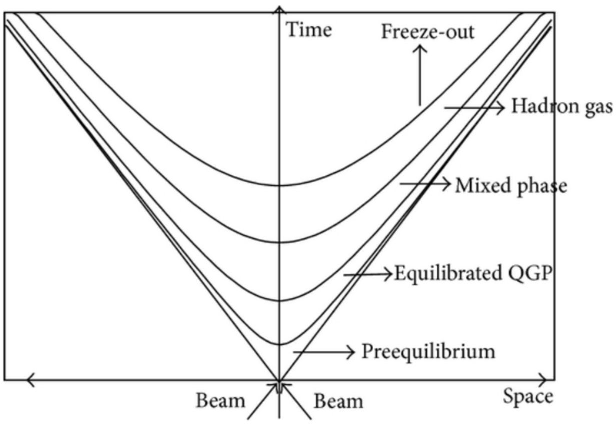

Figure 1.2: Schematic diagram showing the space time evolution of different stages of the heavy ion collisions

The schematic space time evolution of the different stages in a heavy ion collision is constructed out of rigorous theoretical as well as experimental investigations into the heavy ion collisions phenomenon. There are different stages at which the aggregate properties of the debris that comes out of a heavy ion collisions are significantly distinguishable depending on the macroscopic as well as microscopic aspects of the system. The following stages depict the entire space-time evolution of a heavy ion collision.

1.1.1 Initial state and pre-equilibrium

For t<0, two highly energetic beams of ions approach each other bound for collision with some impact parameter b.The ions are at extremely high speed so in the lab frame the nuclei appear as flat discs due to lorentz contraction.At the origin of the space time diagram, That is, at t=0 and z=0, the nuclei either collide non-centrally if the impact parameter is non-zero that is (b $>$ 0) or centrally if the impact parameter is nearly equal to zero (b $\simeq$ 0). In the centre of the collision zone, the nucleons undergo inelastic collisions and a large part of there kinetic energy is deposited and concentrated in a small volume within the collision zone. Within the collision region of the two colliding nuclei, partons (quarks and gluons) are produced in huge amount from the high energy that is concentrated in the overlap region of the colliding nuclei[2].

1.1.2 Thermalization

The highly energetic quarks and gluons created during the initial stages of the heavy ion collision start interacting with each other. The typical mean free path of the strongly interacting matter is much smaller compared to the size of the system. The quarks and gluons undergo subsequent interactions for a typical time period of about for τ= 0 fm/c to τ = 1 fm/c ,finally, the quarks and gluons achieve a state of thermal equilibrium forming a quark gluon plasma. Due to outward pressure gradient,the QGP expands and cools downs within the time period of 3 fm/c to 5 fm/c.

1.1.3 Hadronization and Freeze-out

After the formation of the QGP, as the fireball expands due to outward pressure gradient, the energy density starts falling down and once the energy density falls below the critical value of around 1 GeV/fm^3, Hadronization starts taking place. Expansion continues in the hadronic phase until all inelastic collisions within the system cease to occur. This is known as "chemical freeze-out" as no new particles are created beyond this point in the timeline of the evolution of heavy ion collisions and the chemical composition becomes fixed. As the system further expands,it cools down and after some time it reaches kinetic or thermal freeze-out. The thermal freeze-out is the point in temperature when the density of particles with eleastic cross section σ becomes so small that the mean free path $\lambda = 1/(n\sigma)$ becomes significantly large compared to the size of the system. The transverse momenta of the particles become fixed and the hadrons fall on the detectors freely unaffected by the other debris of the collision. The lifetime of the fireball depends on the collision beam energies. For beams with small energy, it takes more time for two nuclei to completely overlap as compared to for the case when the colliding beams have extremely high energy.The lifetime of fireball can vary from 10fm/c to 15fm/c depending on the beam energy. The particles with larger v_z in the center of mass frame are younger than the particles with smaller v_z because of time dilation. Therefore, the space time evolution of heavy ion collision is expressed in terms of longitudinal proper time $\tau = \sqrt{t^2 - z^2}$ instead of the lab time t. The local fluid velocity is $\sim z/t$ and the local proper time is constant as a result the τ surfaces that envelop the several dynamic regions are approximately hyperbola. The lifetime of the fireball is very small and there is no technology at the current moment that can explore and observe the properties of the fireball directly. However there are still indirect ways to gain insight into the internal properties of the QGP medium. We can study the debris that comes out of heavy ion collisions and study their distribution to understand and probe the properties of the QGP medium that is supposedly formed during early stages of the heavy ion collision.

1.2 Thermal Dileptons and the temperature of the QGP

Now in the heavy ion collisions, it is expected that QGP will form after initial pre-equilibrium state. Now we cannot directly observe the temperature of the QGP state directly as the lifetime of the fireball is very small. So we need to have probes which can give us indirect information related to the temperature of the QGP state[3]. Therefore we need to look for particles that come out of the QGP state after thermalization,without interacting much with the strongly interacting matter within the QGP, hence carrying direct information related to the temperature in the QGP state. That means the probes must have large mean free path (λ) and hence small interaction cross-section(σ) since $\lambda \propto 1/\sigma$

Now hadrons are strongly interacting and hence they have large interaction cross-section leading to small mean free path. Hence,they are not the ideal probes for determining the temperature of the QGP as their momentum distribution deviates from the thermal distribution as they interact via strong interaction as the fireball expands. So, the other possible probes for determination of temperature are electromagnetic probes,that is,real or virtual photons and leptons or dilepton pairs since they don't interact strongly with the QGP medium and hence carry the information related to thermal properties of the QGP to the detectors without much error. Now photons and dileptons are produced during the entire evolution of the heavy ion collision[4]. They interact via the electromagnetic force and even under extreme temperatures and baryon densities achieved in heavy ion collisions, the typical mean free path of the photons is of the order of $10^2 fm - 10^4 fm$ which is much larger than the size of the fireball, hence once they are created, they come out almost without interacting with the strongly interacting surrounding matter.Photons are created in the pre-equilibrium stage, in the QGP phase, in the hadronic phase and from the hadrons produced at freeze-out that decay to give off photons. The photons are categorized as direct photons or decay photons depending on their production mechanism. Direct photons are produced directly from particle collision whereas decay photons come from mostly hadron decay. Depending on the origin, direct photons can be classified into following categories:-

1.) The prompt photons, which originate during the initial hard scatterings.As they are produced in the initial hard processes, prompt photons have a very high p_T.

2.)pre-equilibrium photons, produced before the medium gets thermalized.The momentum distribution of these photons donot follow a thermal distribution

and hence the invariant mass distribution of these photons donot follow a thermal distribution.
3.)thermal photons from quark- gluon plasma as well as from hadronic reactions during the hadronic phase. The momentum distribution of these photons follow according to a thermal distribution and hence, The invariant mass distribution of these photons follow a thermal distribution.
4.)passage of jets through plasma also leads to creation of photons.

Now the main mechanism by which thermal dileptons are produced in the QGP state is that a quark and an anti-quark, which are in thermal equilibrium in the hot fireball annihilate each other to produce an off-shell virtual photon,which further decays into a pair of thermal dileptons. The reaction is shown as follows:-

$$\overline{q} + q \rightarrow \gamma^* \rightarrow l^+ + l^-$$

This is the exact mechanism for production of Drell-Yan dileptons in which a quark from one nucleon annihilates an antiquark from another nucleon to produce a virtual photon which further decays into a pair of dileptons. However, the momentum distribution of Drell-Yan dileptons depend on the annihilating quark and anti-quark whose momentum in turn depend on the nuclear structure function. However, for the thermal dileptons coming out of the QGP, the momentum and hence the invariant mass distribution follows a thermal distribution as the initial annihilating quark and antiquark pair are in thermal equilibrium in the medium. So the Drell-Yan dileptons are different from the thermal dileptons with respective to the fact that Drell-Yan dilepton invariant mass distribution follows a nuclear structure function while the invariant mass distribution of thermal dileptons follow a thermal distribution function. Now, the initial four momentum of the quarks and gluons in the QGP cannot be directly related to the four momentum of the colliding nuclei as the hadron wave function is disturbed during the collision. As the QGP is formed, the quarks and gluons constituting it exchange energy and momentum and reach thermal equilibrium. Now, the QGP consists of both fermions and bosons. The fermions in thermal equilibrium follow the fermi-Dirac statistics and hence the invariant mass distribution of fermions is proportional to the fermi-Dirac distribution function. That is

$$\frac{dN}{dM_{inv}} \propto \frac{1}{exp(M_{inv}/T)+1}$$

Hence, the probability of finding a fermion in some invaiant mass range becomes closer and closer to the fermi-Dirac distribution function as the size of the invariant mass range becomes infinitesimally smaller.

Similarly, the bosons in thermal equilibrium inside the QGP follow the Bose -Einstein statistics and hence the invariant mass distribution of bosons is proportional to the Bose-Einstein distribution function. That is

$$\frac{dN}{dM_{inv}} \propto \frac{1}{exp(M_{inv}/T)-1}$$

Hence, the probability of finding a boson in some invaiant mass range becomes closer and closer to the Bose-Einstein distribution function as the size of the invariant mass range becomes infinitesimally smaller.

However, the temperature of the QGP is extremely high, and in the high temperature limit both the Fermi-Dirac as well as the Bose-Einstein distribution can be approximated by the classical Maxwell-Boltzmann distribution as

$$exp(M_{inv}/T) >> 1$$

Hence, the invariant mass distribution of the thermalized medium and hence the invariant mass distribution of thermal dileptons is proportional to the Maxwell-Boltzmann distribution function,that means

$$\frac{dN}{dM_{inv}} \propto exp(-M_{inv}/T)$$

Here, T is the space-time averaged temperature of the QGP and not the instantaneous temperature. Which means the temperature is calculated at each point and at each time and the average value obtained is this temperature T. So if we obtain the invariant mass distribution of the thermal dileptons coming out from QGP and make an exponential fitting to it, then the slope of the exponential fit will give the inverse of the temperature. Hence, we can find the space-time average temperature of the QGP by taking inverse of this slope. In this project, we will be constructing the invariant mass distribution of thermal di-muons to get an estimate of the QGP temperature. This analysis will be done using the MUCH detector in the CBM experiment. Much detector is optimized to construct invariant mass distribution of Di-muons.The thermal dileptons are produced in all mass range, However, in the invariant mass range below 1 Gev/c^2, the dimuon invariant mass spectra is dominated by dimuons coming from the decay of hadronic resonance states like ρ, ω and ϕ. In the mass range above 3 GeV/c^2, the dimuon spectra is dominated by high mass states like j/ψ and higher mass resonances. Hence, the mass window between 1 GeV/c^2 to 3 GeV/c^2 is free from all the resonant background muons and is ideal for getting the information related to temperature measurement of the QGP. There are ofcourse background dimuons coming from decay of hadronic resonances,kaons and pions as follows:-

$\pi^+ + \pi^- \rightarrow l^+ + l^-$

there are also background from dalitz decay like:-

$\pi^0 \rightarrow \mu^+ + \mu^- + \gamma$

$\eta \rightarrow \mu^+ + \mu^- + \gamma$

There are also backgrounds from decay of D mesons.

Also, the dimuon spectra from the hadronic phase dominates the dimuon spectra from the QGP phase in the mass range below 1 GeV/c^2. Also, higher the transverse momentum of the dimuons, the more is the possibility that the dimuons are from the early stages of the QGP. Hence, selecting a suitable p_t and mass range for the dimuon spectrum, we can analyze it's invariant mass to obtain the QGP temperature. The slope of the thermal distribution,that is, the inverse temperature, will change with time as the temperature will decrease due to expansion of the fireball. With the decrease in temperature, the contribution to the thermal dilepton invariant mass distribution at that temperature will become less,hence the slope will increase in magnitude. So there will be minimal contribution near freeze-out. Hence, as the temperature of the quark gluon plasma is the greatest, so the mass contribution to the thermal dileptons during the QGP phase will be maximum. Since the invariant mass distribution is independent of the frame of reference, the temperature obtained is independent of the collective motion of the fireball.

Chapter 2

The CBM Experiment

The Compressed Baryonic Matter (CBM) experiment, has been planned, at the accelerator facility FAIR at GSI,darmstadt and is aimed at the production and scientific exploration of extremely dense nuclear matter in laboratory conditions.The CBM experiment is capable of exploring the QCD phase diagram of nuclear matter in the region of intermediate temperatures and extremely high baryonic densities. By colliding atomic nuclei at relativistic energies,it is possible to artificially create hot and dense nuclear matter over a wide range of temperatures and densities .At extremely high temperatures or densities the hadrons melt resulting to the formation of Quark Gluon Plasma. This is in contrast with other high energy physics experiments like in LHC, QGP is made at high temperature and densities.The CBM experiment is designed for detection and measurement of rare observables which have very low production cross-sections using the high-intensity heavy ion beams produced by the FAIR accelerators and it is comprised of various components designed and developed to specifically measure a particular type of observable.

2.1 Basic Science behind Muon Identification in CBM Experiment

The entire idea behind particle identification in the CBM experiment is that the system consists of layers of absorbers and detectors. The absorbers are capable of absorbing the hadrons that come out as debris from the heavy ion collision. The fundamental factor behind hadron absorbtion capabilities of a hadron absorber is the hadron interaction length λ_I. This is also called the nuclear interaction lenght.λ_I can be defined for a particular medium as the average distance that a hadron will traverse inside the medium before it experiences a nuclear interaction inside the medium. The hadron interaction length is given by :-

$$\lambda_I = \frac{A}{N_A \sigma_i \rho}$$

Here A is the atomic mass number of the absorber, σ_i is the cross-section of inelastic collision between a nucleus of the absorber medium and the incident hadron, N_A is the avogadro's number and ρ is the density of the absorber medium. Hence, smaller is the hadron interaction lenght, more is the hadron absorbtion capability of the detector and vice versa. One of the major challenge that the CBM experiment must overcome is that it should be able to distinguish and detect the low momentum muons in a region of high particle density. The low momentum muons may arise from decay of low mass vector mesons and they will not have very high energy. Now particles, when they pass through a material medium can experience multiple scattering due to interaction with the medium. If the muons that pass through the detectors and absorbers experience multiple scattering frequently, that means their initial momentum when they came out of the fireball is disturbed. That would mean that the track reconstruction of the muons will be affected severely by the absorbers resulting in poor mass resolution. Hence our detector system must be optimized to have large radiation lenght so muons can pass experiencing minimum multiple scattering but at the same time it must also have small hadron interaction length so that most of the hadrons get absorbed. Now the radiation length goes as $X_0 \propto A/Z^2$,where Z is the atomic number. The scattering angle is connected to the radiation length according to the following law:-

$$\theta_0 = \frac{13.6}{\beta p} z(\sqrt{z/X_0}[1 + 0.038 \ln{(x/X_0)}]$$

where β, ρ and z are the velocity, momentum and charge number of the incident particle, and $\frac{x}{X_0}$ is the thickness of the scattering medium in units of radiation lengths.

Keeping all this under consideration, the material for hadron absorbers have been selected through simulation for different heavy ion collisions and passing their debris through the detector system to get the estimates that which material best suites our requirement for detecting low momentum muons in a region of high particle density, while at the same time also capable of detecting high momentum muons coming from decay of high mass resonance like j/ψ.

2.2 Details of the CBM Experiment

The CBM experiment consists of the following components:-

2.2.1 Dipole magnet:

The dipole magnet is the source of the magnetic field that influences the initial particles produced during the collision.The field region is confined within 1 m along the beam axis to restrict the size of the tracking detectors located inside the field.It has a large aperture of 25 polar angle, and provides a magnetic field integral of 1 Tm.Superconducting coils will be used to meet cost efficiency.

2.2.2 Micro-Vertex Detector (MVD):

MVD has excellent position resolution as the primary objective of MVD is to determine the decay vertices of open charm particles by meeting the criteria of minimized multiple scattering.very low material budget is also always preferable . These requirements are met by Monolithic Active Pixel Sensors (MAPS). The MVD consists of 3 MAPS layers located at 5, 10, and 15 cm downstream of the target in the vacuum and hence has a compact structure.

2.2.3 Silicon Tracking System (STS):

The primary objective of STS is basically to track the motion of charged particles in the magnetic field. The objective is to determine event multiplicity and track reconstruction. To determine the momentum of the charged particles from the track curvature ,The system will be operated in the magnetic field. It consists of 8 tracking layers of silicon detectors covering the aperture between the polar angles 2.5 and 25 degrees . They are located at distances between 30 cm and 100 cm inside the magnetic dipole field downstream of the target.

2.2.4 Ring Imaging Cherenkov Detector (RICH):

The primary objective of RICH detector is to identify electrons and suppress pions in the momentum range below 10 GeV/C.This will be achieved using a gaseous RICH detector build in a standard projective geometry with focusing mirror elements and a photo detector. It will consist of a 1.7 m long gas radiator and two arrays of mirrors and photo detector planes.The mirror plane is split horizontally into two arrays of spherical glass mirrors, 4×1.5 meter squared each[5].

2.2.5 Muon Chamber System (MUCH):

The primary experimental challenge for measurement of muons in heavy ion collisions at FAIR energies is to identify low-momentum muons within an environment having high particle densities. In the CBM experiment,the concept is to track the particles through a hadron absorber system, and to perform a momentum-dependent muon identification.To realize this concept,the hadron absorber is segmented in several layers and triplets of tracking detectors planes are placed within the gaps between the absorber layers. The absorber/detector system is placed downstream of the Silicon Tracking System (STS) which determines the particle momentum.The absorber/detector system has to be as compact as possible In order to reduce meson decays into muons . The actual design of the muon detector system consists of 6 hadron absorber layers (carbon 60 cm, iron plates of 2 20 cm, 30 cm, 35 cm and 100 cm thickness) and 18 gaseous detector planes located in triplets behind each absorber slab. The momentum of a muon varies with the mass of the vector mesons and with beam energy.This enables us to make muon identification based on momentum

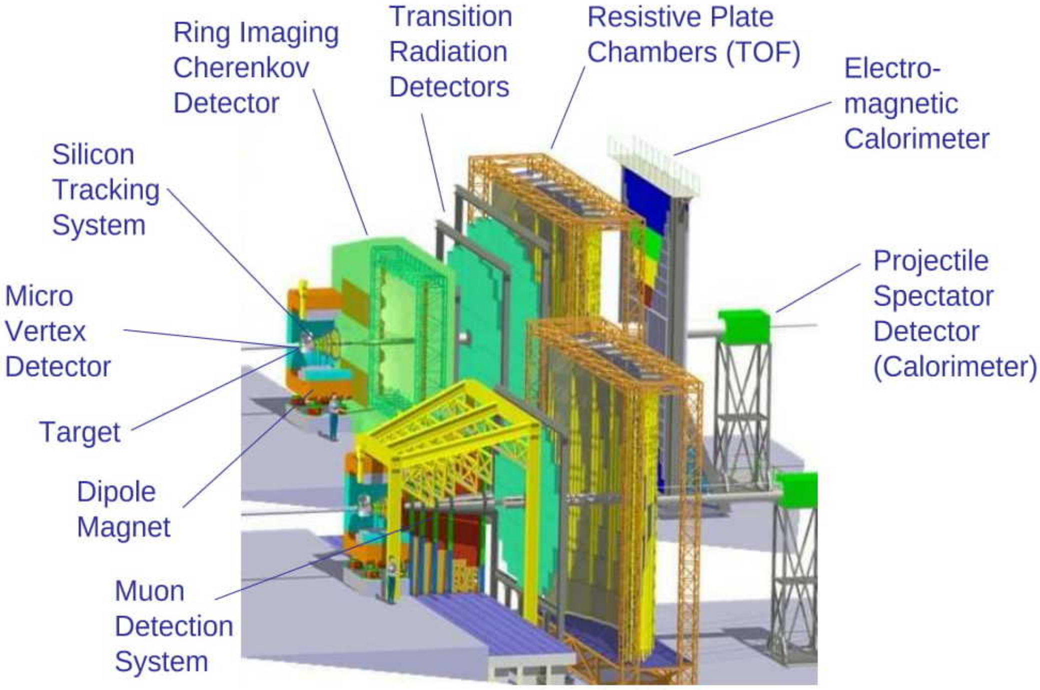

Figure 2.1: Details of the CBM Experiment

analysis. The challenge for the muon detectors and for the track reconstruction algorithms is the very high particle densities of up to a maximum of 0.3 hits/cm^2 per central event in the first detector layers after 20 cm of iron. The numbers are down by a factor of 4 in case of minimum bias collisions. Hence rate of 10 MHz this hit density translates into a hit rate of 0.75 MHz/cm^2 minimum bias collisions.

2.2.6 Transition Radiation Detector (TRD):

Each detector station consists of 3 detector layers which ensure particle tracking and identify electrons and positrons.TRD consists of three such detector stations.The total active area of the detector amounts to about 600 m^2 .The detector stations are located at approx- imately 5 m, 7.2 m and 9.5 m downstream of the target.

2.2.7 Timing Multi-gap Resistive Plate Chambers (MRPC):

It is an array of Resistive Plate Chambers.This will basically be useful for identification of hadrons through TOF measurements.The active area covered by TOF will be about 120 m^2 and it will be situated at about 6 m downstream of the target for measurements at SIS100 energies , and at 10 m at SIS300 energies. The necessary time resolution is of the order of about 80 ps [9].

2.2.8 Electromagnetic Calorimeter (ECAL):

In heavy ion collisions, photons might be produced right at the beginning of the collision or photons may also be produced due to neutral mesons, decaying into photons.so calorimetry will be used to measure these photons.Direct photons can give us a measurement of the temperature of QGP.The ECAL consist of modules which consistituted from 140 layers of 1 mm lead and 1 mm scintillator,each with with cell sizes of 3×3 cm^2 , 6×6 cm^2 , and 12×12 cm^2 . The shashlik modules can be accommodated either like a wall or in a tower like geometry with variable distance from the target.

2.2.9 Projectile Spectator Detector (PSD)

To determine the collision centrality and the orientation of the reaction plane,The PSD will be used.The PSD is a completely compensating modular lead-scintillator calorimeter that is designed to obtain very good and uniform energy resolution. The calorimeter is made from 44 individual modules, each consisting of 60 lead/scintillator layers having a surface area of 20×20 cm^2. The scintillation light is read out by wavelength shifting (WLS) fibers by Multi-Avalanche Photo-Diodes (MAPD) that have an active area of 3×3 mm^2 and a pixel density of $10^4/mm^2$.

2.3 Details of the various components of the MUCH Detector

In order to investigate the conditions inside the QGP fireball with dimuons, we develop a MUCH (Muon chamber) system which is able to identify muon pairs in a wide range of beam energies, from low energies at SIS100 up to top SIS300 energies.

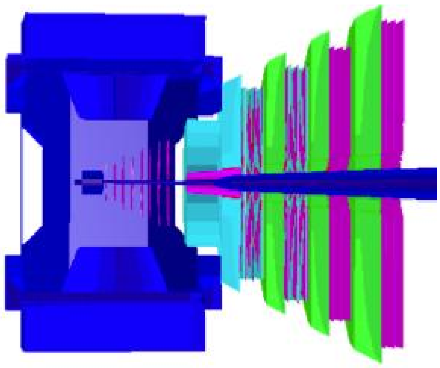

Figure 2.2: Schematic view of the MUCH SIS100-B configuration. It consists of 12 detector layers and 4 absorbers including the first absorber of 60cm carbon

The MUCH concept requires up to six detector stations, each station consisting of 3 layers. Each layer can therefore be considered as one tracking layer consisting of detectors built using specific detector technology.The sis100-B version of the MUCH system has a carbon absorber of thickness 60 cm and 3 iron absorbers with a total thickness of 70 cm.It consists of 4 absorbers and 12 detector layers.

2.4 Details of the Detectors within the MUCH System

Now each tracking station in the MUCH system basically has 3 detector layer. The covered active area of each layer has been divided into trapezoidal sector-shaped modules. Each module is arranged on a support structure, of around 2 cm thickness. Detector modules are attached at the front and the back sides of the support structure and filled with Argon based gas mixture as the active medium. Even though the technologies differ from one station to the other, all stations will however have gaseous detectors of different technologies. This allows us to use gas as sensitive medium in the simulation throughout. The Argon gas used as active medium has thickness of 3 mm.The distance between the chamber centers is 10 cm to provide enough space for accommodating the detector profile that includes electronics boards, mechanics, cooling arrangement among others. A 2 cm overlap of the sensitive volume is kept along the radial direction to avoid the dead zone. The number of sectors in a particular detector plane depends on the radii of the station. Half of the total set of sectors are arranged in the front face and rest half in the back face. The number of sectors that can be accommodated in a detector layer is a tunable parameter. MUCH aims to study the propagation of tracks inside the segmented absorbers. The study of geometry therefore involves the implementation of conical absorbers of varying sizes placed around the conical beam pipe. Conical absorbers are used to accept the forward focused particles. The detector modules are of trapezoidal profiles that are placed behind each absorber block. For effective tracking, each tracking station consists of 3 layers of tracking chambers. Each tracking layer consists of a thin support structure and an equal number of sector-shaped modules are placed on two faces of the support structure.

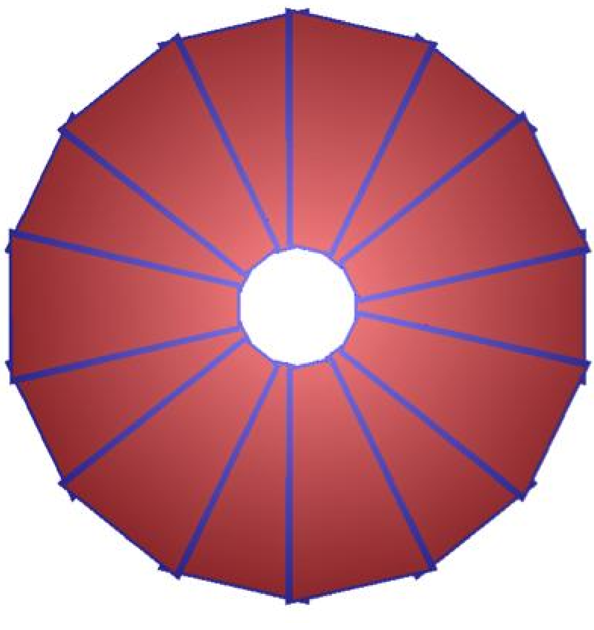

Figure 2.3: Schematic view of the layout of the muon chambers with trapezoidal overlapping sectors

For reducing the dead-space, modules on two faces are placed in such a way that a border of the module on one side has overlap with an active zone of the module on the opposite side. The number of stations, their shape, size and number of modules are varied for optimization of efficiency and signal to background ratio (S/B) for detecting low-mass vector mesons and charmonia. For building a detector, one or more GEM foils separated by spacers of suitable thicknesses are placed inside a gas tight enclosure filled with suitable gas mixture. The enclosure usually consists of two PCBs. The gap between the top PCB and first GEM foil forms the drift gap. Incoming radiation produces primary ionization in this region. This is followed by subsequent drift of the electrons through the GEM holes which act as amplifying elements. The gap between the last GEM foil and bottom PCB forms the induction or collection gap. Signals due to electrons are collected by the readout electrodes placed on the inner copper layer of the PCB at the bottom of the induction gap. In most of the cases, GEM detectors use a gas mixture of Ar and CO_2 in the ratio of 70:30. This gas mixture makes the detector insensitive to neutrons.

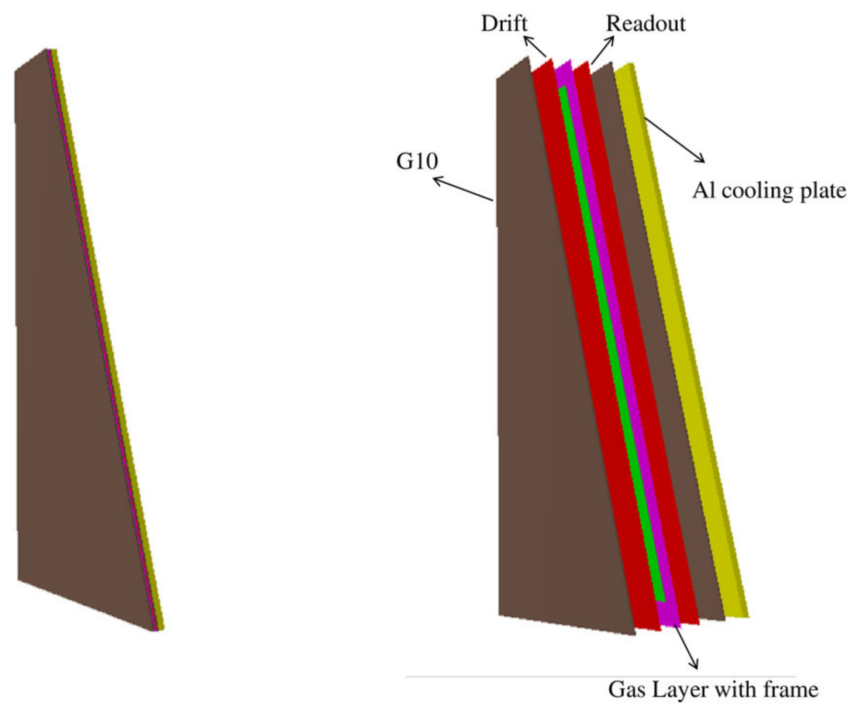

Figure 2.4: Details Of the trapezoidal section of a detector layer with PCB

Chapter 3

ANALYSIS 1

Now the version v17b of the MUCH detector setup does not includes the effects of PCB on the momentum as well as on the transverse momentum distributions of the primary and secondary particles that are produced as they interact with the material of the detector.However the version v18a of the MUCH setup includes the effects of PCB on the momentum and transverse momentum distribution of the primary and secondary particles.In this project,a comparison has been made between the momentum distribution of primary as well as secondary particles at the third layer of first and second station of the MUCH setup for version v17a and v18b.further comparison has also been made for the momentum and transverse momentum distribution for the entire MUCH system for both version v17b and v18a.Comparison of momentum and transverse momentum distribution for primary and secondary particles has been done for the complete MUCH detector. Then a comparison of momentum and transverse momentum distribution for all particles has been done for MUCH v17b and MUCH v18a versions. Then a comparison of primary and seconday pion momentum and transverse momentum distribution has been done for MUCH v17b and v18a versions of the complete MUCH detector. And finally the momentum and transverse momentum distributions of primary and secondary protons have been obtained and compared for complete MUCH setup with versions v17b and v18a respectively. The analysis has been done within the CBM ROOT framework.

3.1 Analysis of momentum and transverse momentum distrbution of primary and secondary particles

Au-Au collisions at 12 GeV minimum bias condition are simulated within the CBM root framework[7]. 100000 events have been simulated for this analysis. The event generator UrQMD have been employed to generate these event particles. The transport code GEANT3[6] has been employed and momentum and transverse momentum distributions for the primary and secondary particles at the third layer of station 1 and station 2 have been obtained and compared for v17b and v18a of the MUCH detector setup respectively. The following figures show the comparison of the respective plots obtained for v17b and v18a version of the MUCH setup.

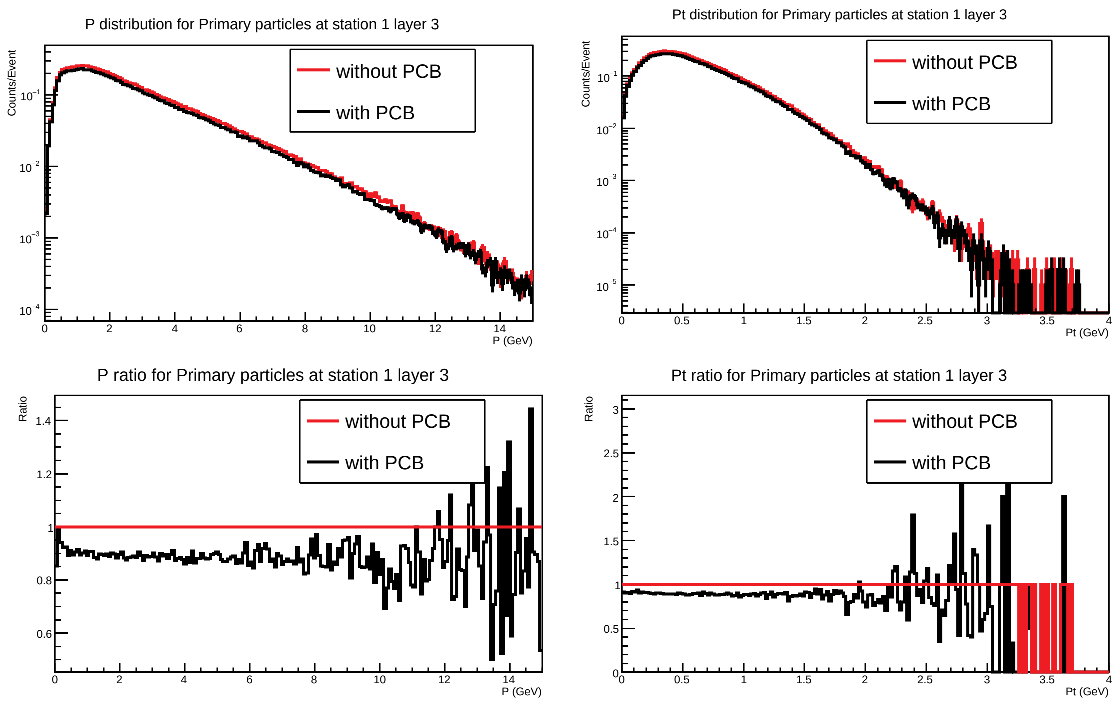

Figure 3.1: P and Pt distribution comparison at station 1 layer 3 for primary particles

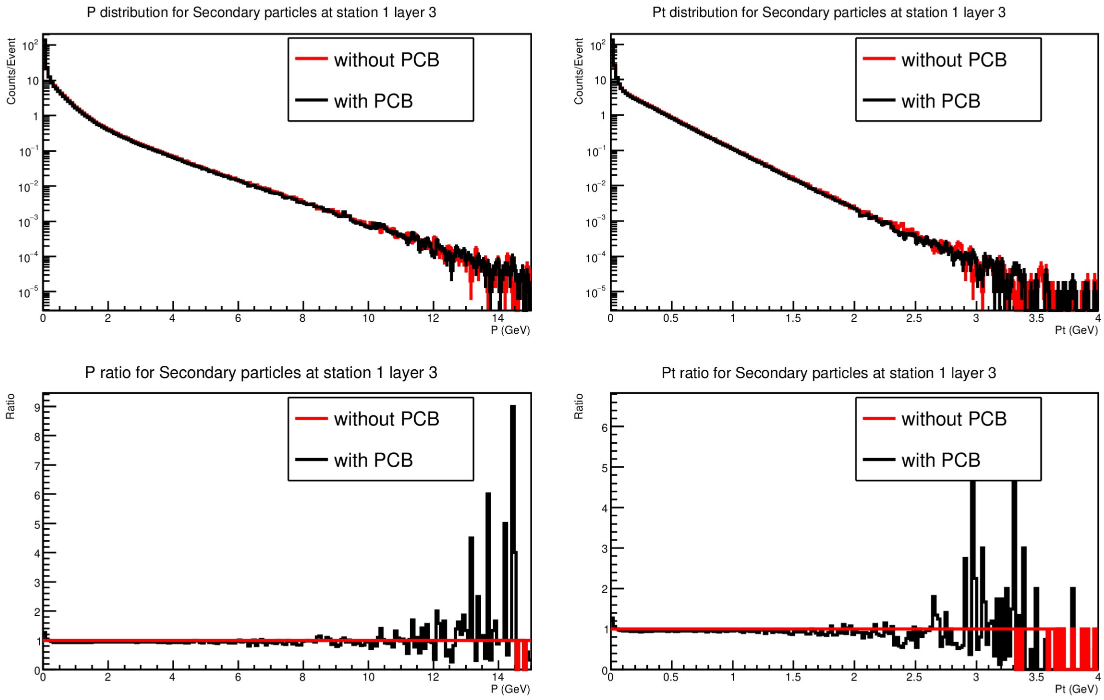

Figure 3.2: P and Pt distribution comparison at station 1 layer 3 for secondary particles

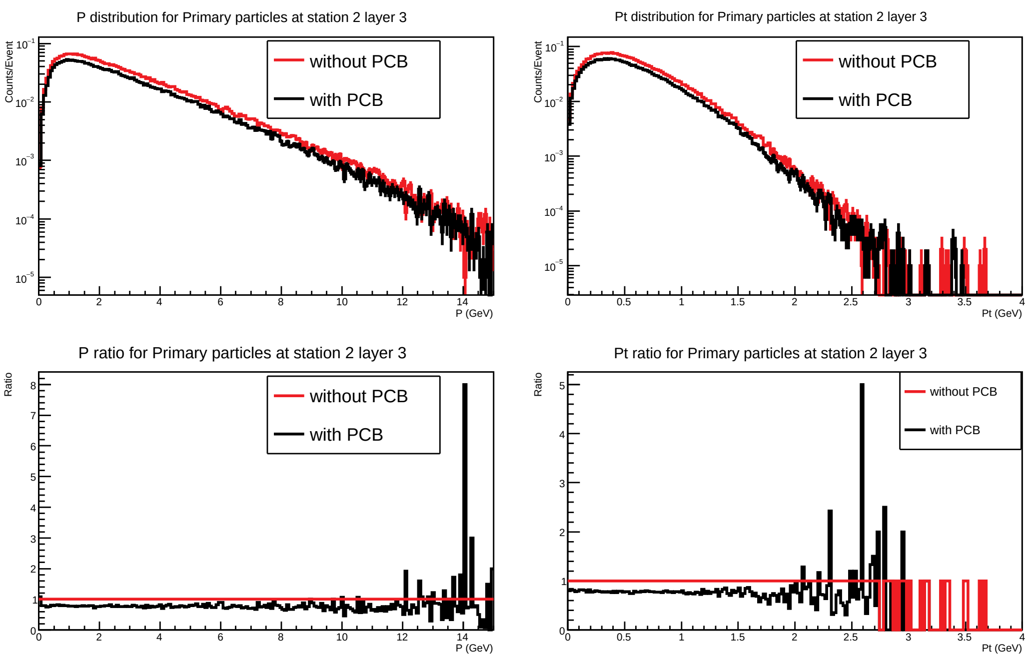

Figure 3.3: P and Pt distribution at station 2 layer 3 for primary particles

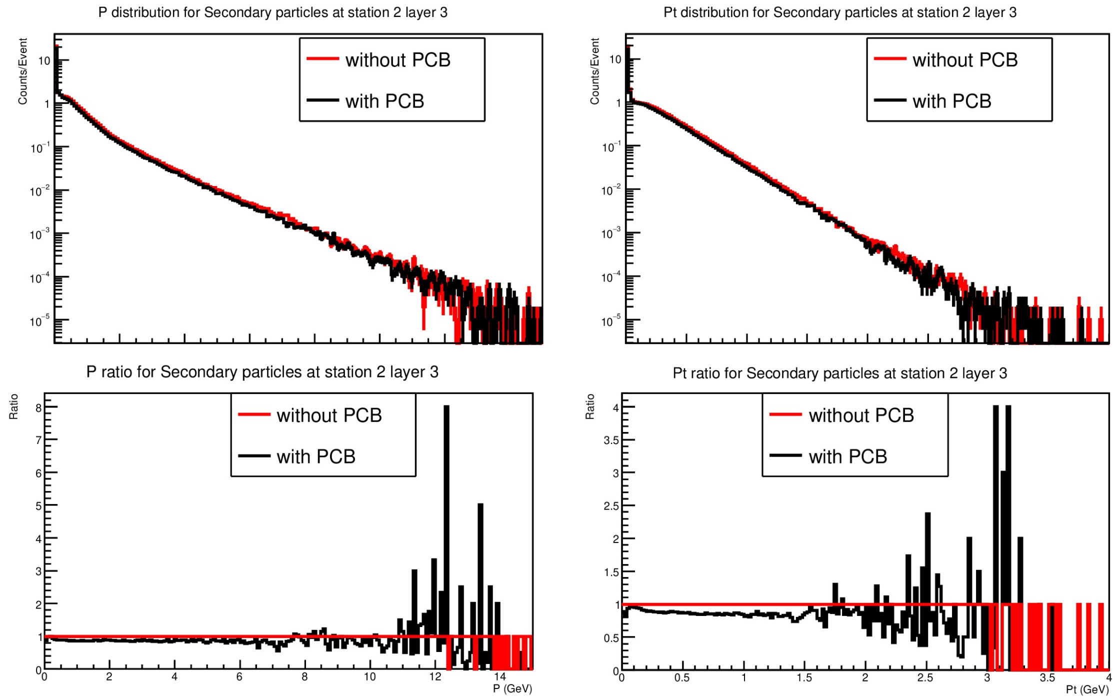

Figure 3.4: P and pt distribution at station 2 layer 3 for secondary particles

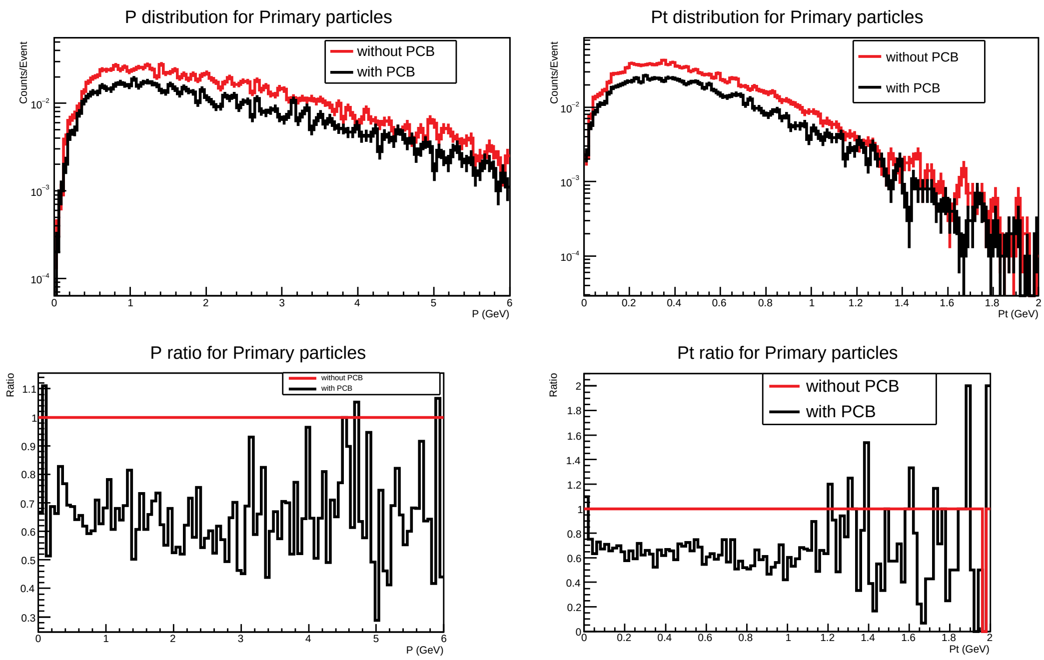

Figure 3.5: P and Pt distribution of primary particles for the entire MUCH system

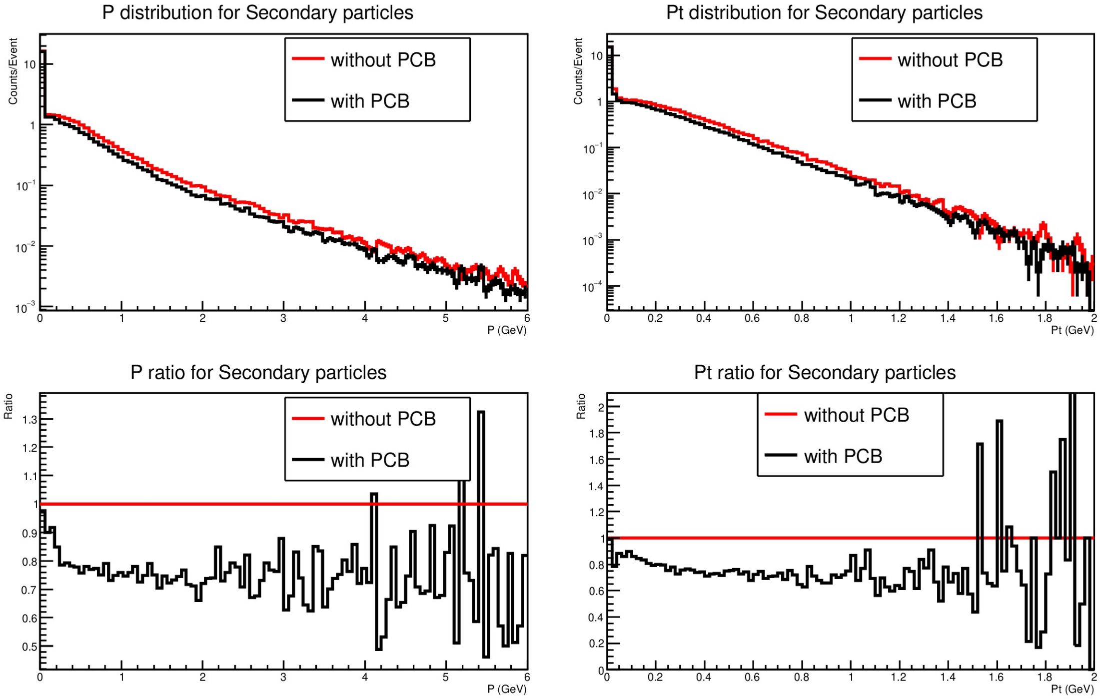

Figure 3.6: P and pt distribution for secondary particles for the entire MUCH system

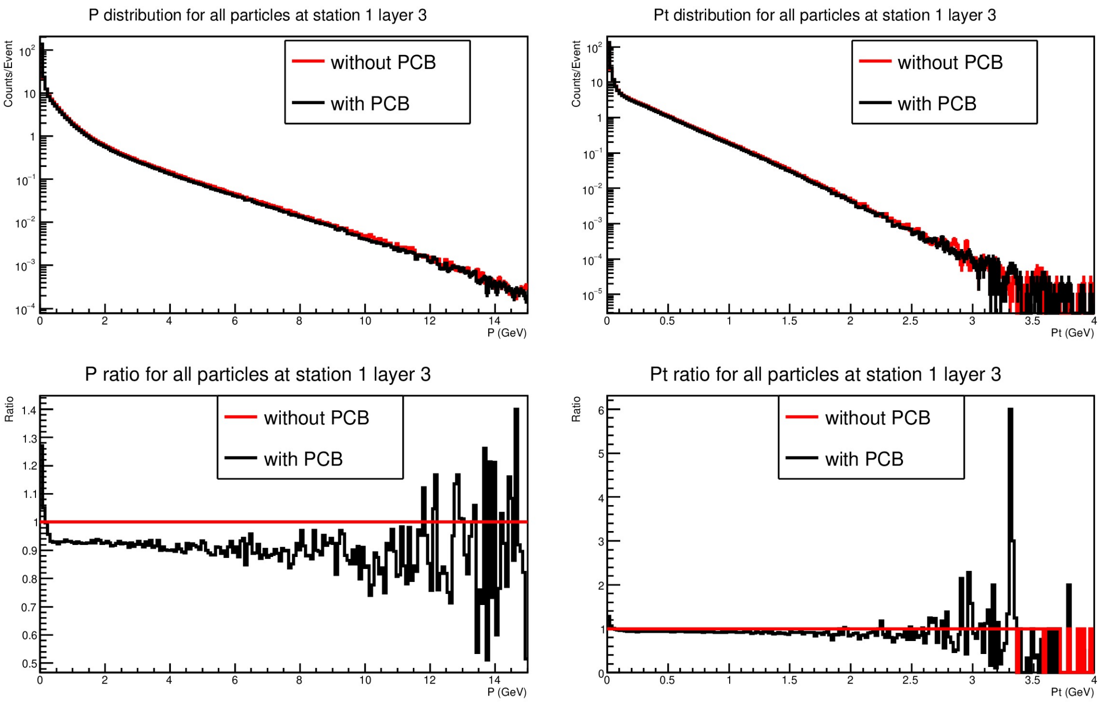

Figure 3.7: P and pt distribution for all particles at station 1 layer 3 of the MUCH Detector.

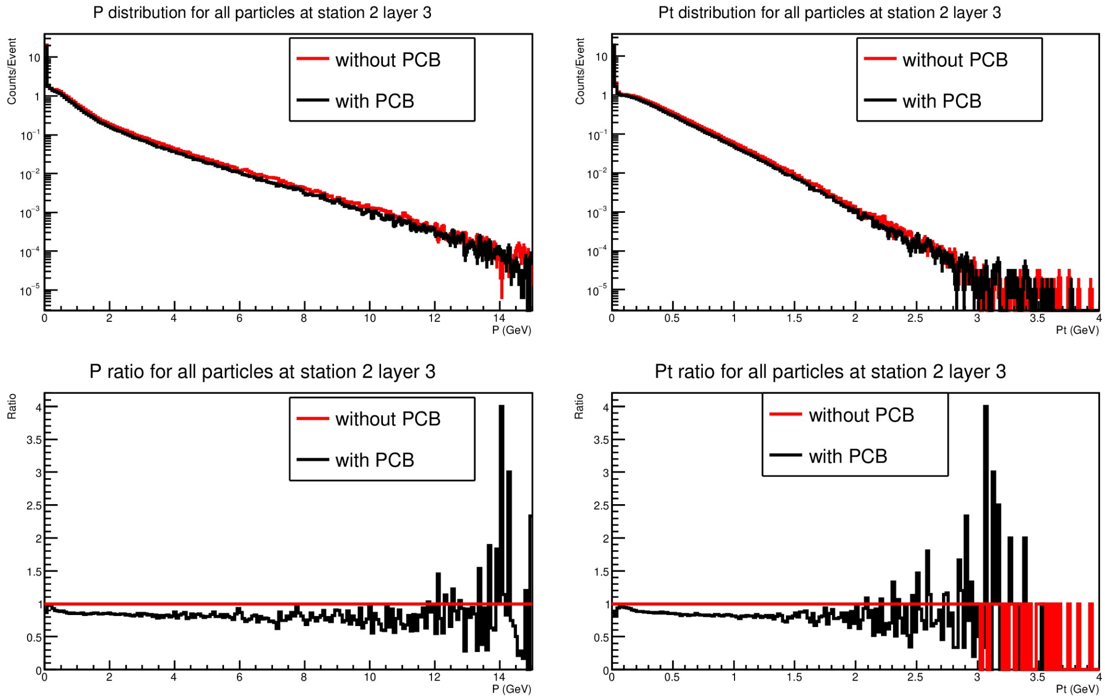

Figure 3.8: P and pt distribution for all particles at station 2 layer 3 of the MUCH Detector.

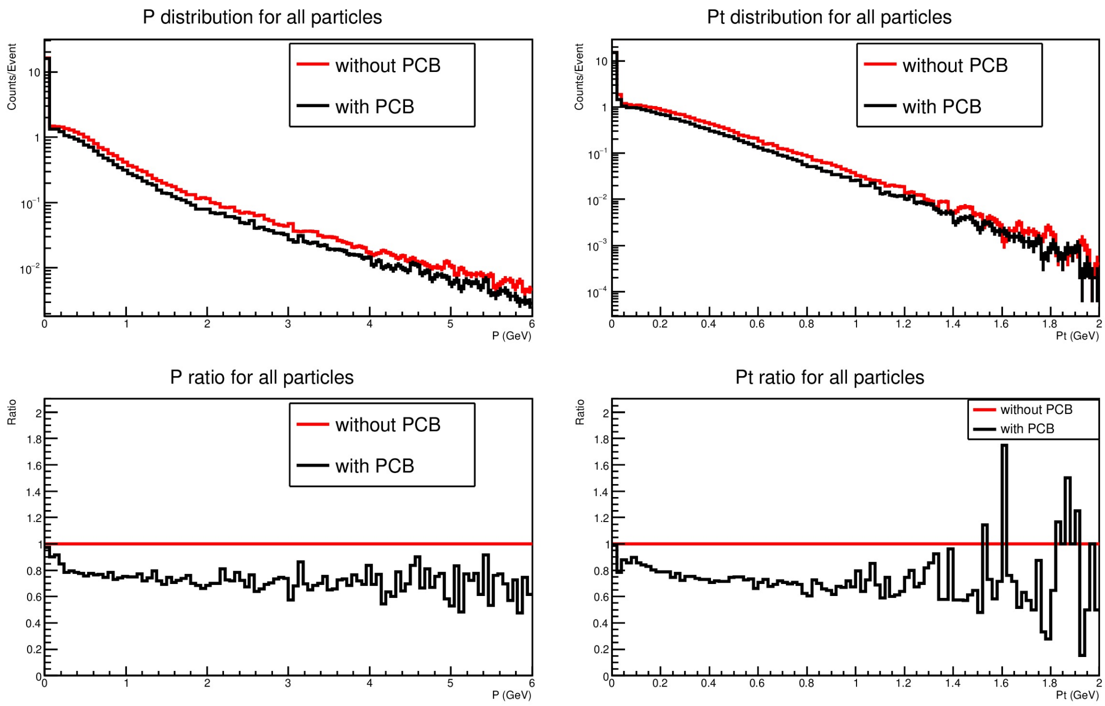

Figure 3.9: P and pt distribution for all particles for the entire MUCH Detector.

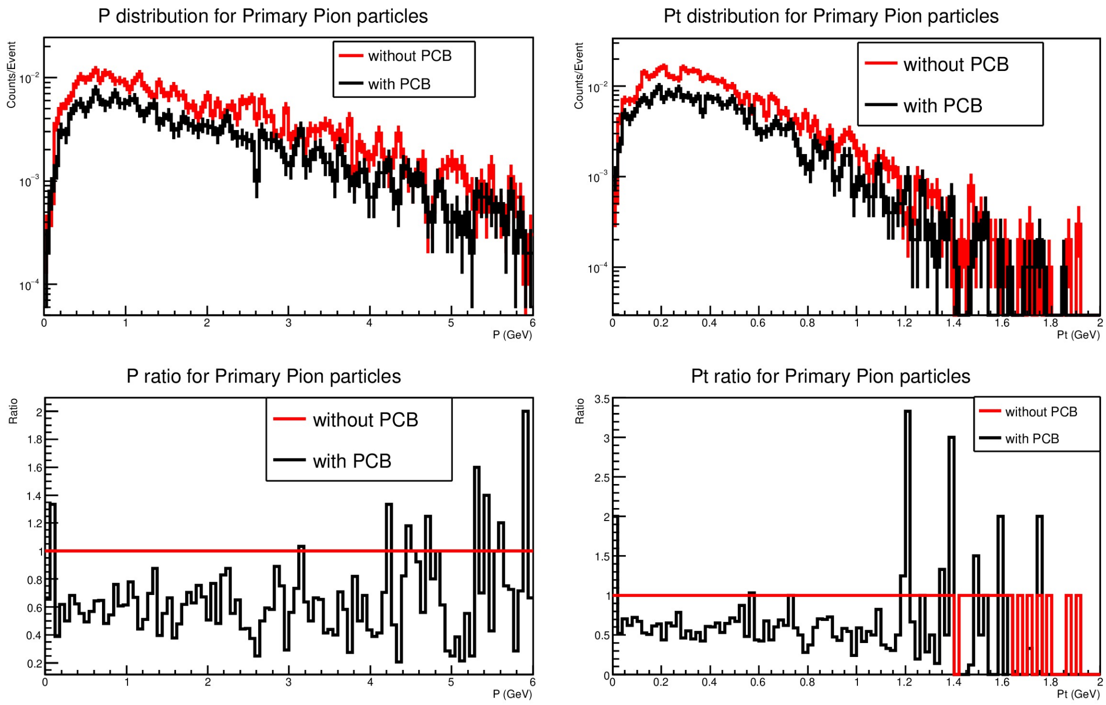

Figure 3.10: P and pt distribution for primary pion particles for the entire MUCH Detector.

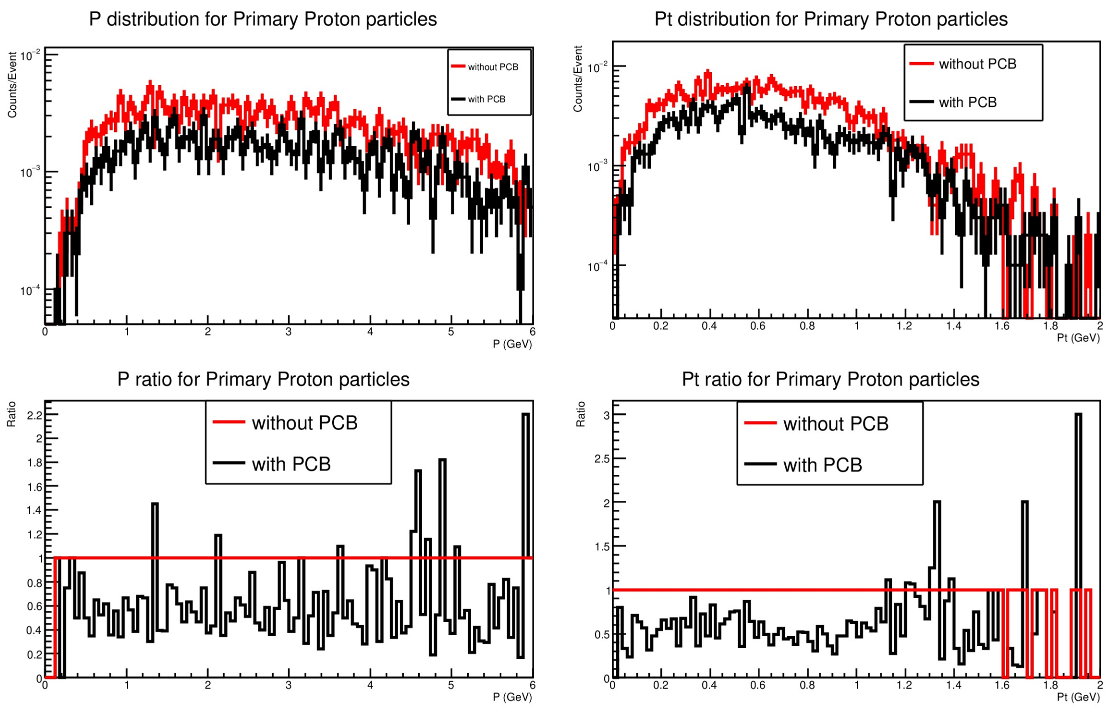

Figure 3.11: P and pt distribution for primary proton particles for the entire MUCH Detector.

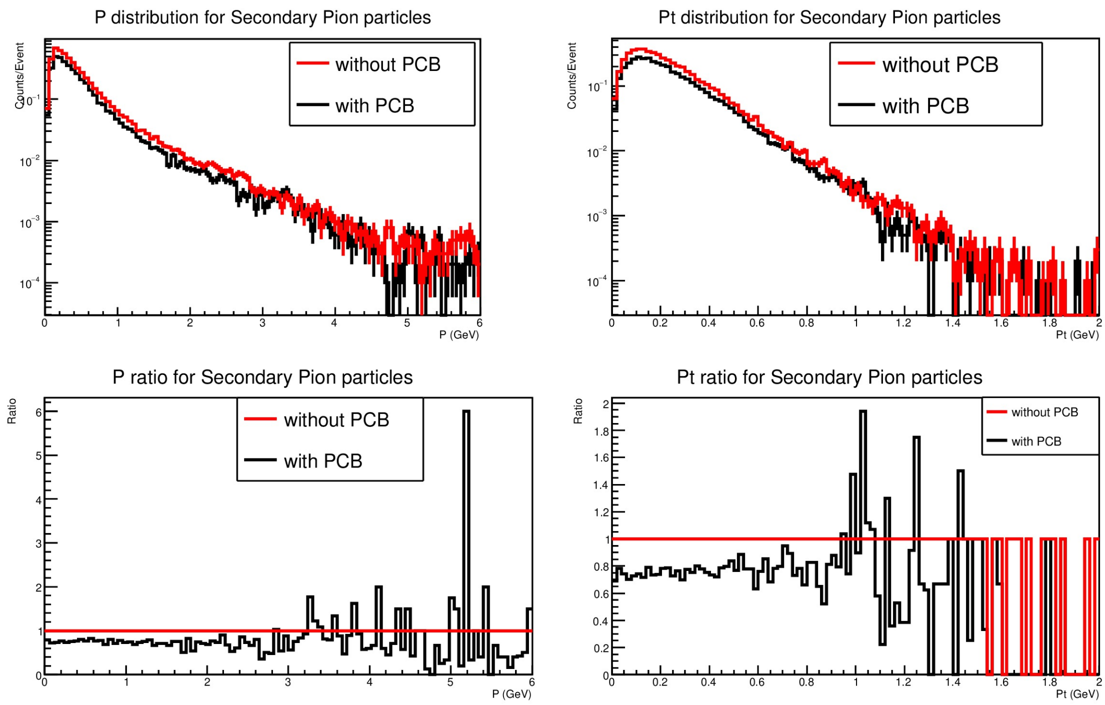

Figure 3.12: P and pt distribution for secondary pion particles for the entire MUCH Detector.

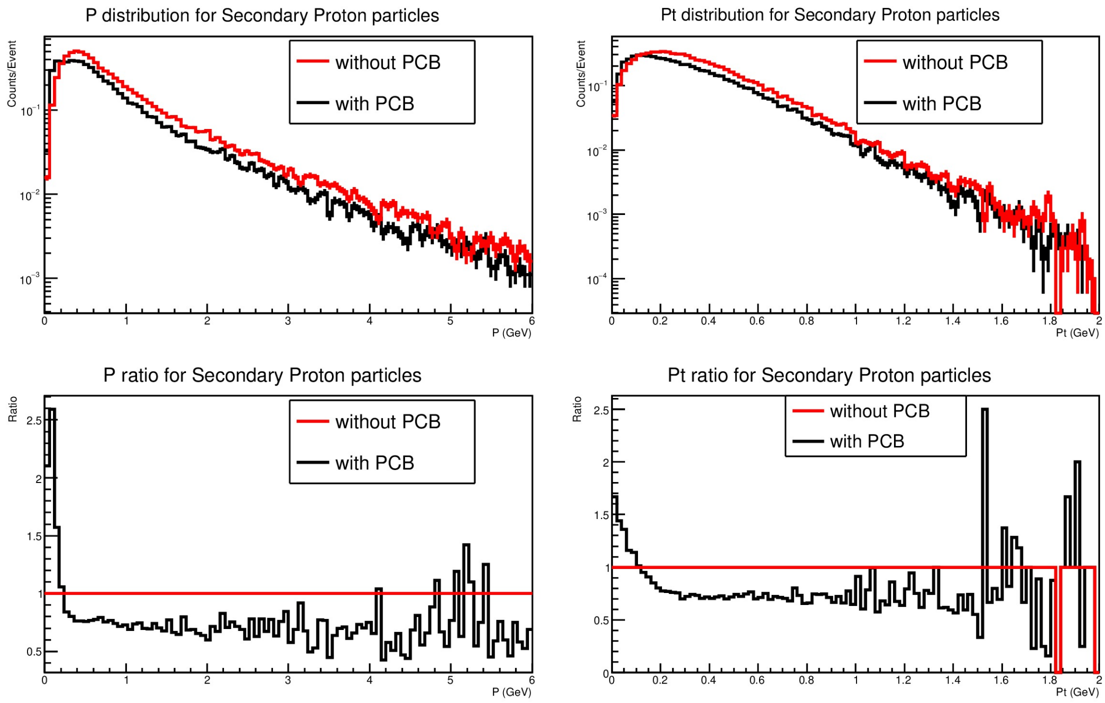

Figure 3.13: P and pt distribution for secondary proton particles for the entire MUCH Detector.

3.2 Conclusion

From the above analysis,it is found that there is slight decrease in the value of momentum (P) as well as transverse momentum (Pt) distributions due to employement of PCB into the detector setup. Lesser number of primary particles are observed since the PCB absorbs a small fraction of the primary particles.However,the number of secondary particles increase as is expected since the initial particles from the collision will interact with more matter as they pass through the entire detector setup. With introduction of PCB into the detector system, the number of production of secondary particles will increase significantly, since there is more matter with which the collision debris can interact to produce secondary particles. However , the energy carried by these secondary particles is pretty low so they will subsequently be also absorbed by the material within the detector system that intersects with their trajectory. Hence, the combined effect is that there is slight decrease in the momentum and transverse momentum distribution of the primary and secondary particles.

Chapter 4

Analysis 2

In the CBM experiment, The QGP that will be produced will be of high baryon density, Which has never been produced and it is essential to study the thermodynamic properties of such high baryon density QGP, So we need to measure the temperature of the QGP and we need to make a simulation study of such an experiment.In this section we will be demonstrating various simulations related to how we can measure the temperature of the QGP formed in the CBM experiment. The need for such a simulation study is very crucial because, the CBM experiment will start at around the year 2025 and we need to optimize the abilities and capabilities of the experimental setup and simulations are efficient, cost effective and they save a lot of time and also give an idea of how will we really interprete the data that will eventually come out when the experiment will finally begin.

All the simulations have been done using the march 2019 version of the CBM Root framework. The version of the MUCH geometry employed for all analysis is v18a. This means that the PCB layer has been attached to the detector in the MUCH setup. The transport code applied to the entire simulation chain is GEANT3. Initially we have simulated 200k thermal dimuons at 8 GeV and obtained the distribution of all it's kinematic variables to get an idea of the properties of the signal thermal dimuons. For this purpose, we have used the PLUTO event generator.The spectral function used by the PLUTO generator to produce particles has been obtained through a microscopic transport model[10]. Next we have obtained the invariant mass distribution of these thermal dimuons and obtained the temperature in the mass range 1 GeV to 2 GeV as this mass region will be dominated by the radiation from the QGP. This has been done without passing the thermal dileptons through the CBM setup. Hence, we can consider this temperature as a reference temperature and we should be getting a temperature close to this value after we pass the thermal dileptons through the entire CBM setup and reconstruct it's invariant mass. Next we have taken the 200k thermal dimuons and simulated them to pass through the CBM setup. The obtained muon hits in the final detector of the MUCH setup have been used to reconstruct the dimuon invariant mass spectra and from this invariant mass spectra we obtain the temperature of the QGP.we have done analysis for the entire p_t as well as also for different p_t ranges. In order to make our simulation more realistic, we must also include the effects of background particles because in a real heavy ion collision, a huge amount of background indeed will be generated. So next we have created the background particles using an event generator called UrQMD. UrQMD produces background particles by calculating the production cross-section as well as the interaction cross section of various particles. It does so using either hydrodynamic models or microscopic transport models depending on the energy of collisions and is applicable from 2 A GeV to 200 A GeV collisions. Here we have considered minimum bias collisions of Au-Au 8 A GeV collisions. The background particles generated are passed through the CBM setup and reconstructed at the final detector of the MUCH geometry. The invariant mass spectra of the background particles are reconstructed for the entire range of p_t as well as for different ranges of p_t. Finally we have taken both the signal thermal dimuons created from the PLUTO[8] event generator as well as the background particles created from the UrQMD event generator and passed them together through the CBM setup. We have obtained the invariant mass distribution of the combined signal and background for the entire range of p_t as well as for different ranges of p_t. Finally we have subtracted the background from the combined signal and background to estimate the capabilities of the CBM setup with respect to temperature measurement of QGP formed in the heavy ion collisions.

We have done all analysis for 200K Au-Au minimum bias collisions at 8 A GeV. We have done all the CBM related analysis using standard cut selction values , The transport code used is GEANT3 and the MUCH geometry that has been used is v18a version of SIS100-B setup. The various conditions used to select muon candidates in the MUCH detector are as follows:-

1.) MUCH hits = 11
2.) STS hits = 7
3.) MUCH χ^2 = 1.3
4.) STS χ^2 = 1.2
5.) Vertex χ^2 = 2

We have fitted the invariant mass spectra with the function

$$f(x) = \exp(\alpha + \beta M_{inv}) \qquad ...(1)$$

Where α just scales the exponential function and the inverse of the magnitude of β gives the effective temperature.

4.1 Analysis of the signal thermal dimuons

In this section we have taken 200k thermal dimuon pairs and obtained the distributions of their various kinematic variables in order to get an estimate of the quality of our signal. This is pure raw signal and the dimuons are not passed through the CBM chain here.

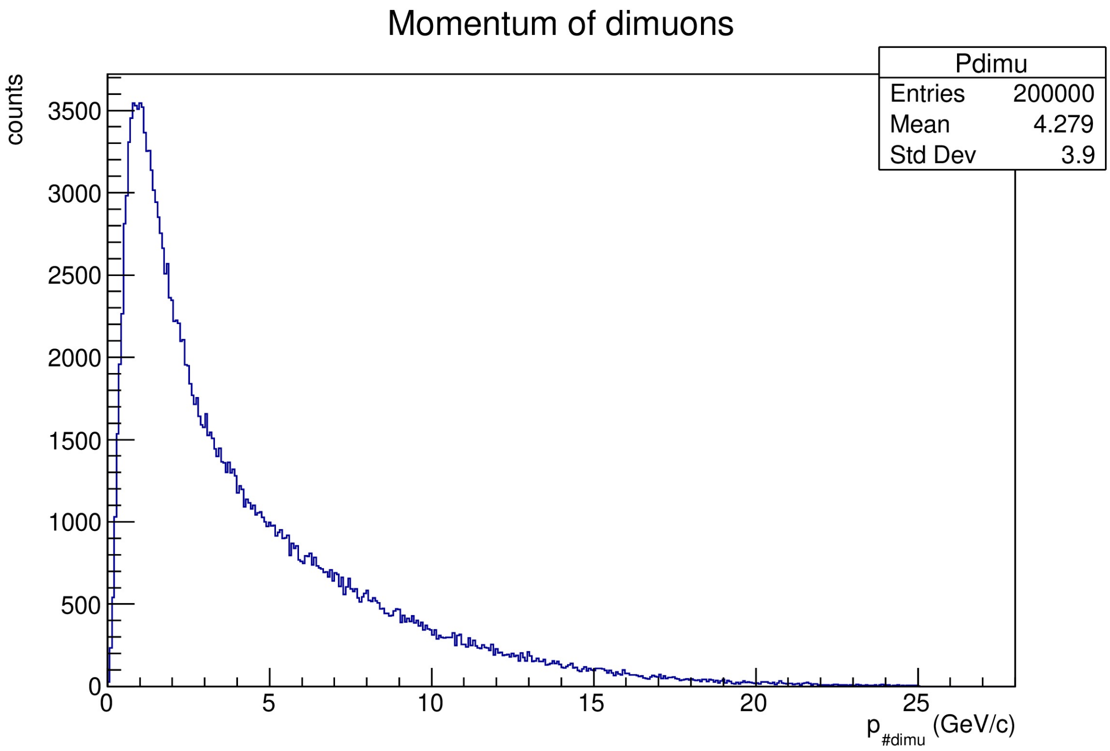

Figure 4.1: Momentum distribution of dimuons obtained using PLUTO

from figure 4.1, We see that initially the momentum distribution rises with momentum (p) then decreases exponentially as it should be the case for boltzmann distribution. The momentum distribution changes with p according to equation (2) as

$\frac{dN}{dp} \propto p * exp(-p/T)$ ...(2)

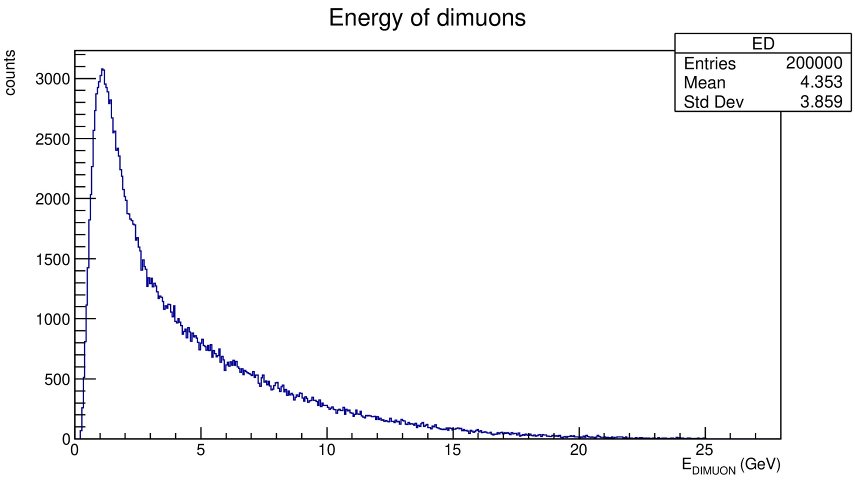

Figure 4.2: The energy distribution of dimuons

In figure 4.2 , we plot the energy distribution of the dimuons and observe that it decreases exponentially with increasing energy as should be the case if Boltzmann statistics is applicable to describe the thermodynamic properties.

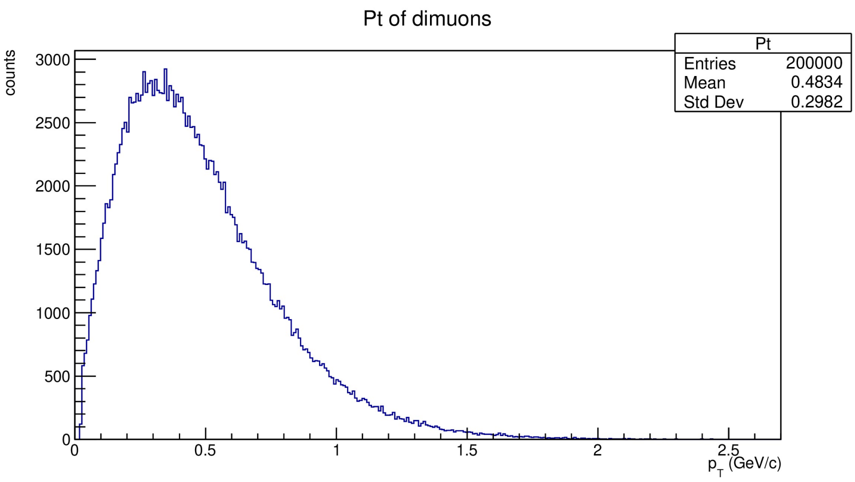

Figure 4.3: Transverse momentum distribution of dimuons obtained from PLUTO

From figure 4.3 we observe that the transverse momentum (p_t)distribution decreases exponentially with increasing transverse momentum.The variation of the transverse momentum distribution with transverse momentum is given by equation (4) as

$$\frac{d^2N}{dp_t^2} \propto exp(-p_t/T) \qquad ...(3)$$

$\frac{dN}{dp_t} \propto p_t exp(-p_t/T)$ ...(4)

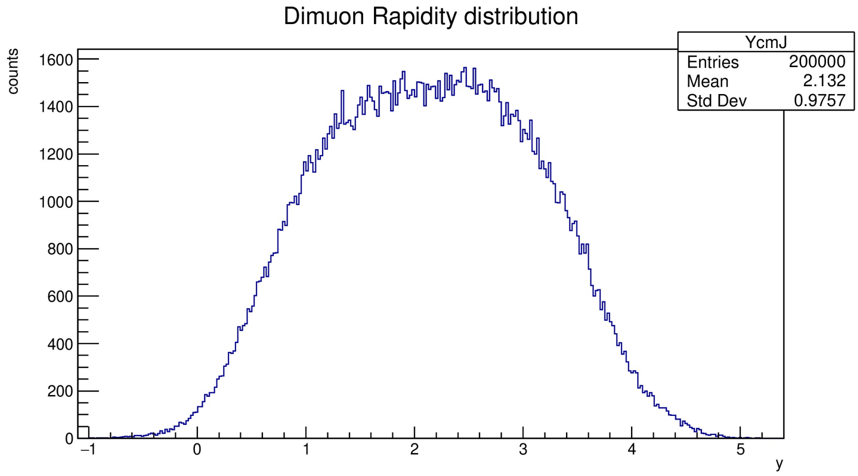

Figure 4.4: The rapidity distribution of dimuons

Now rapidity(Y) of a particle is defined in terms of it's energy-momentum components as

$Y = 0.5ln(\frac{p_0+p_z}{p_0-p_z})$ ...(5)

where p_0 is the energy component of the energy-momentum four vector and p_z is the component of the three momentum along the beam axis. From the rapidity distribution in figure 4.4, We can see that it's shifted towards positive values indicating that it's a fixed target collision between the parent nucleons.

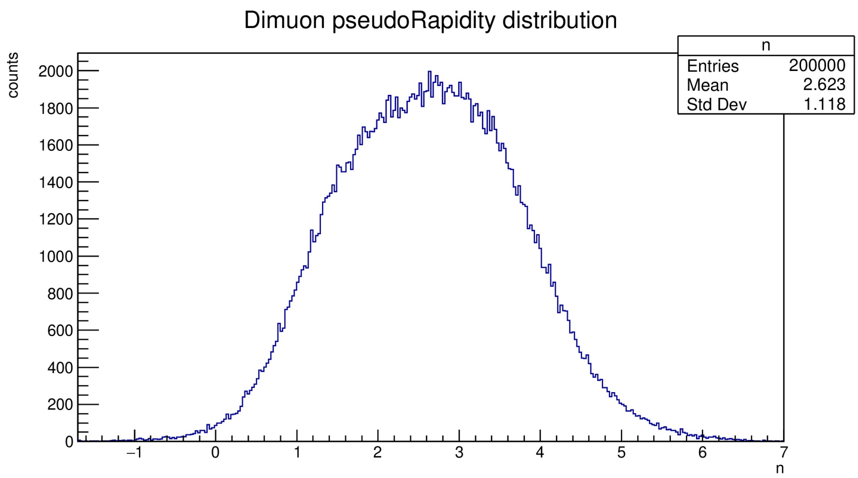

Figure 4.5: The pseudorapidity distribution of dimuons

Now pseudorapidity(η) is a kinematic variable which is much easier to measure as compared to rapidity and nearly equals to rapidity in the high energy limit. It is given by

$$\eta = -ln[tan(\theta/2)] \qquad ...(6)$$

where θ is the angle the emergent particle makes with the beam axis. From the distribution of pseudorapidity from figure 4.5, We can see that it's shifted towards the forward direction indicating fixed target collision between the colliding nucleons.

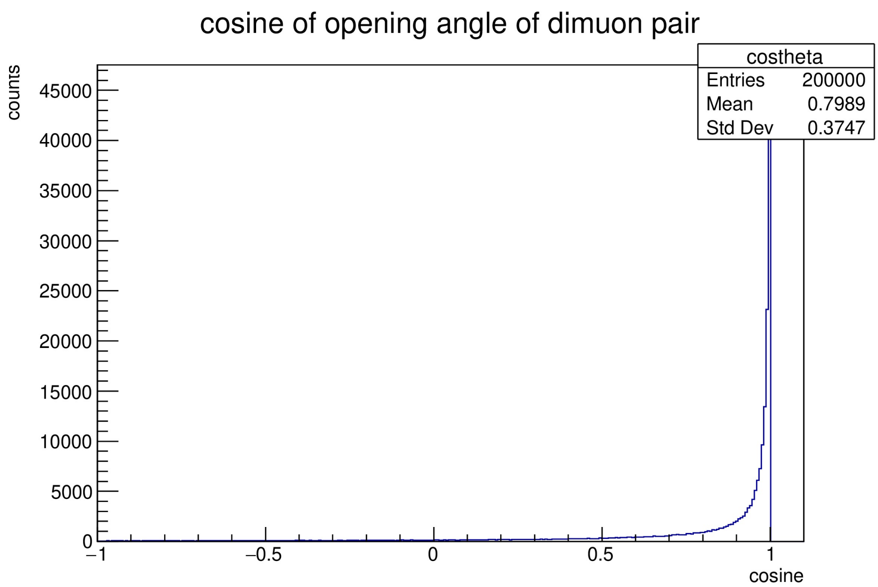

Figure 4.6: The variation of the cosine of the opening angle between two muons in the dimuon

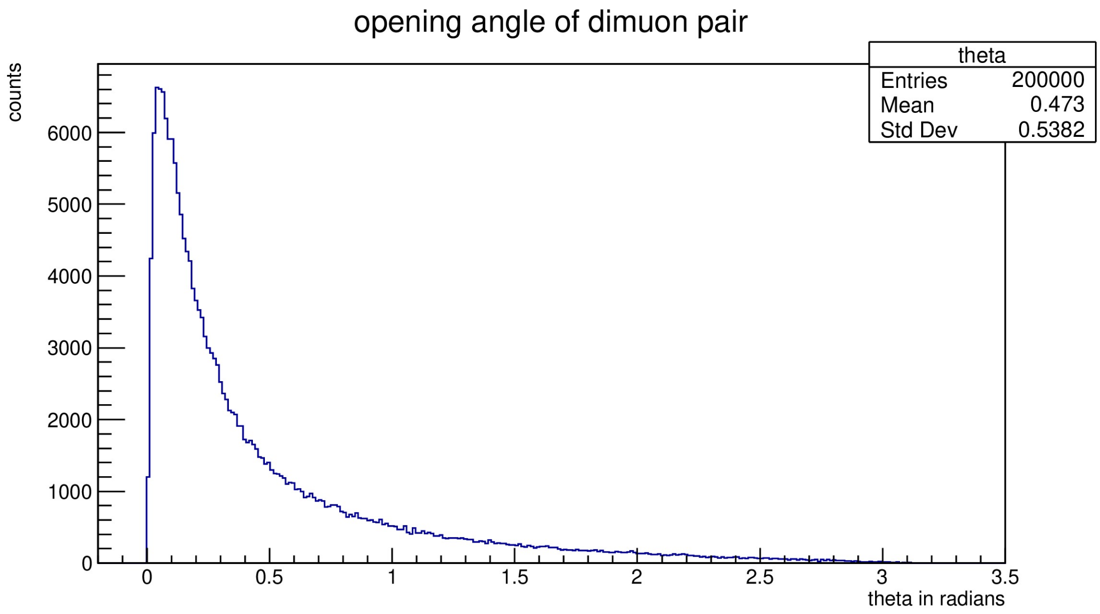

Figure 4.7: The variation of the opening angle between two muons in a dimuon measured in radians

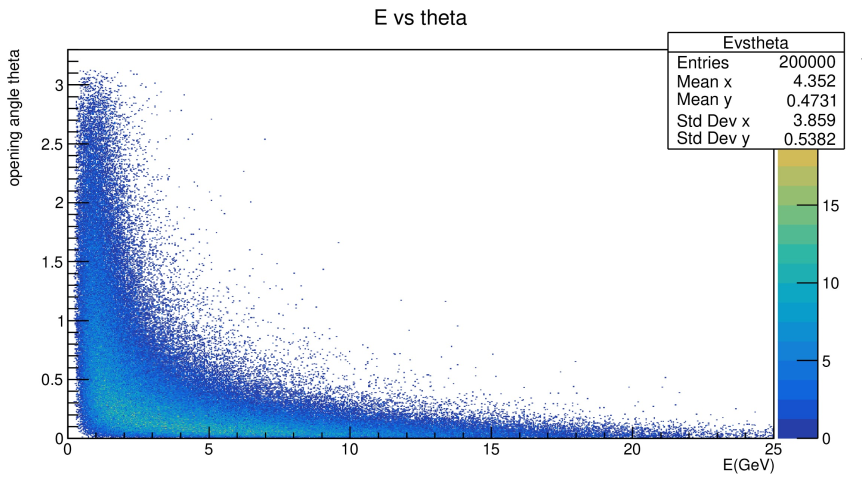

Figure 4.8: The variation of the opening angle with respect to energy

From the distribution for variation of opening angle with energy as shown in figure 4.8, We see that at low energy,many dimuon pairs have large opening angle, but with increase in energy, the number of dimuon pairs with large opening angle decreases, and at very high energy, the dimuon pairs have very small opening angles. This indeed should be the case for fixed target collision as high energy means more longitudinal momentum which would decrease the opening angle.

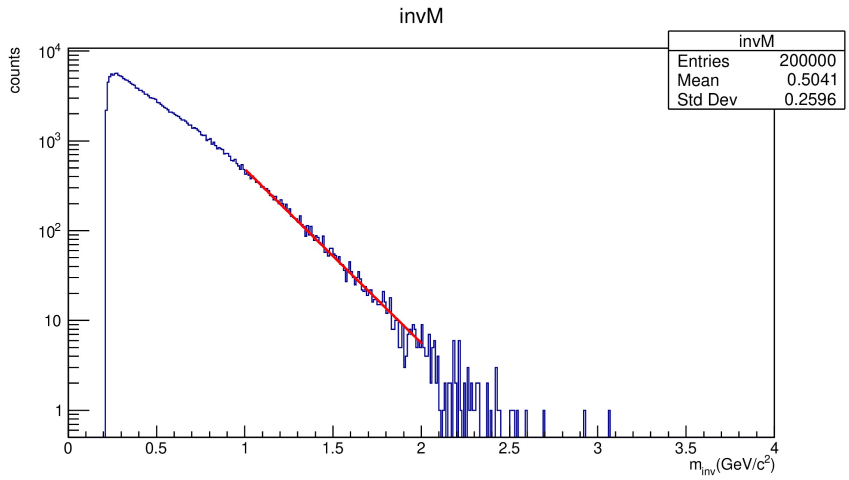

Figure 4.9: invariant mass distribution of signal dimuons

in Boltzmann approximation we have

$\frac{dN}{dM_{inv}} \propto exp(-M_{inv}/T)$ ...(7)

The invariant mass distribution of signal dimuons is plotted in figure 4.9 and the slope of the exponential fit has been obtained to get the reference temperature. Here

α = 10.6400

β = -4.4568

χ^2 = 1.3

The mass range selected for exponential fit is from 1 GeV to 2 GeV. This range is selected as it would be clean from the dimuon spectra coming from other resonance states. From figure 4.9, We find that the reference temperature is, $T_{ref} = 224 \pm 3.36 MeV$.

This temperature is much higher than the threshold temperature of 160 MeV in the low baryon density region of the QCD phase diagram for a transition from a hadronic to partonic phase. Since the initial collision energies are of the order of 8 GeV, hence the QGP created in these events will be in the region of high baryon density as nucleons tend to bind momentarily and time taken for complete overlap of two nuclei is longer as compared for very high energies. And from the QCD phase diagram it is evident that the threshhold temperature for a transition from hadronic phase to partonic phase is much lower, We can expect that these signals are indeed coming from the QGP phase of the heavy ion collision event.

4.2 Analysis of each single muon in the dimuon pair

In this section we have obtained the distributions of various kinematic variables for each signal muon that is a part of dimuon pair. This has been done to get an idea about the kinematic properties of each individual muon .

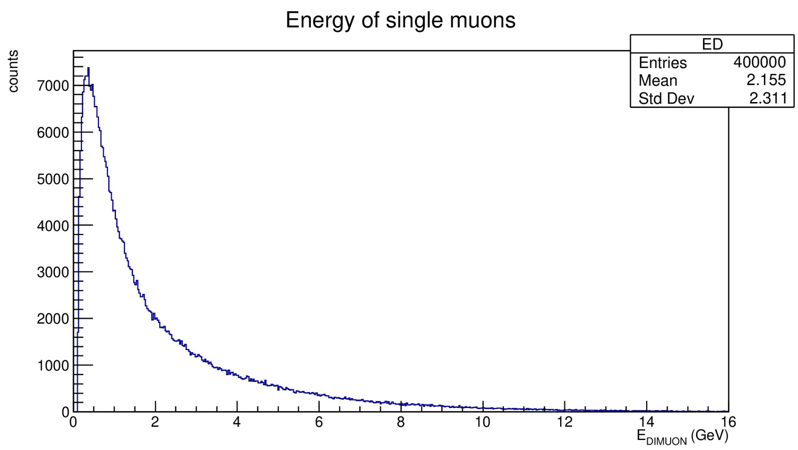

Figure 4.10: The energy distribution for each muon

In figure 4.10, We see that the energy distribution is in accordance with the Boltzmann statistics.

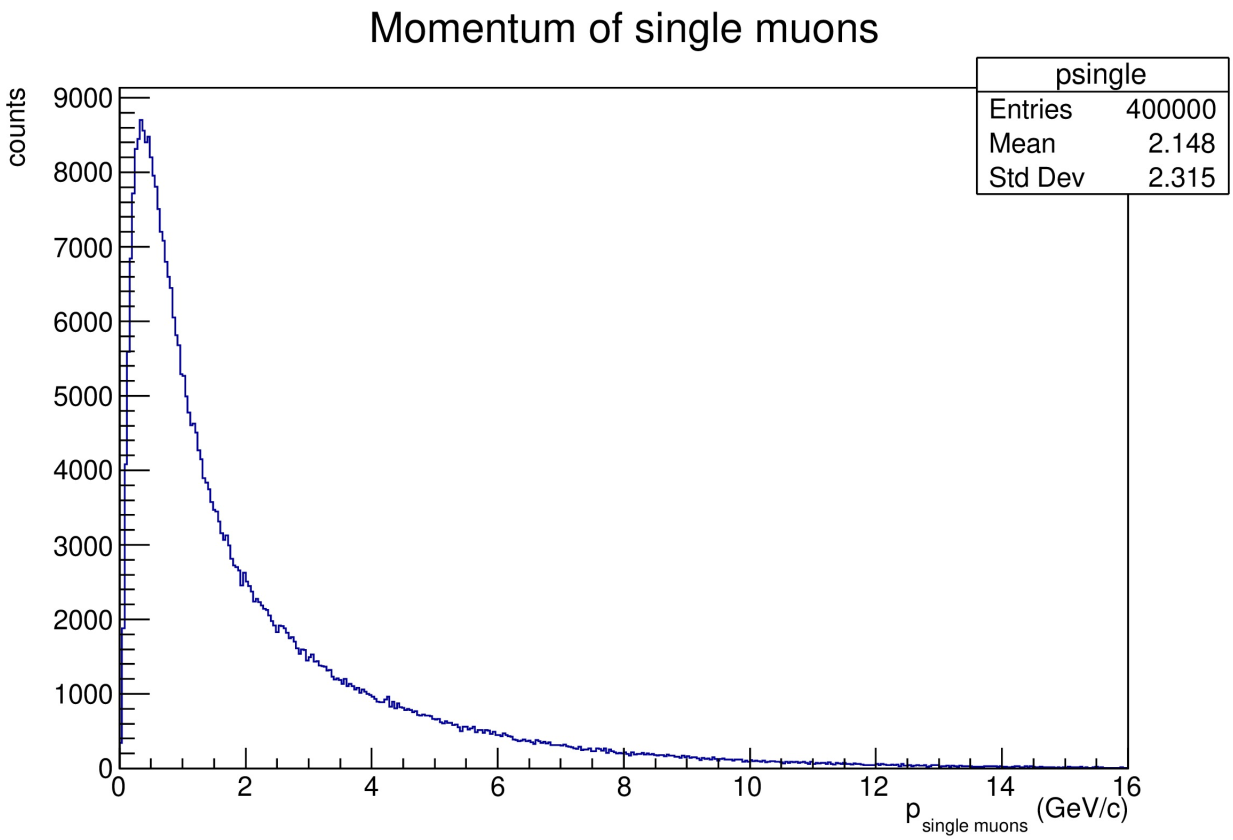

Figure 4.11: The momentum distribution for each muon

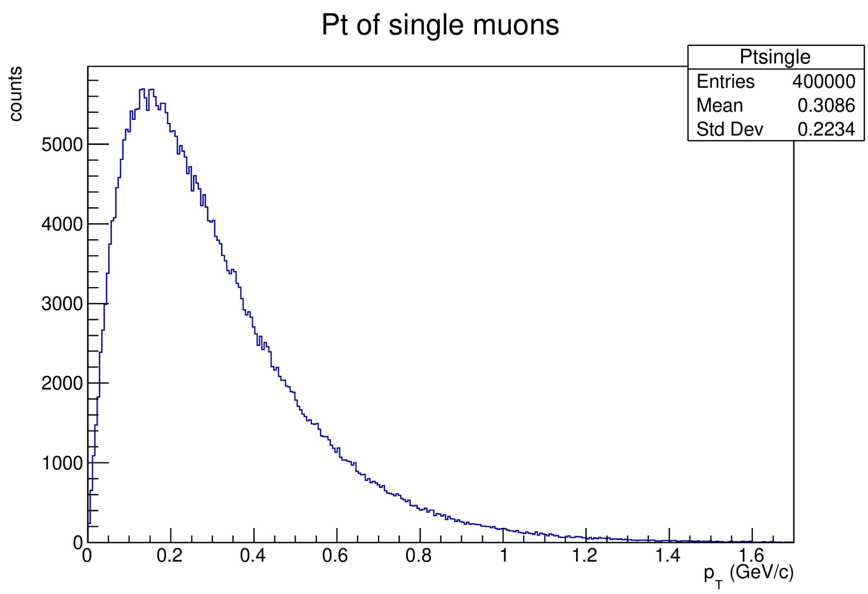

Figure 4.12: The transverse momentum distribution for each muon

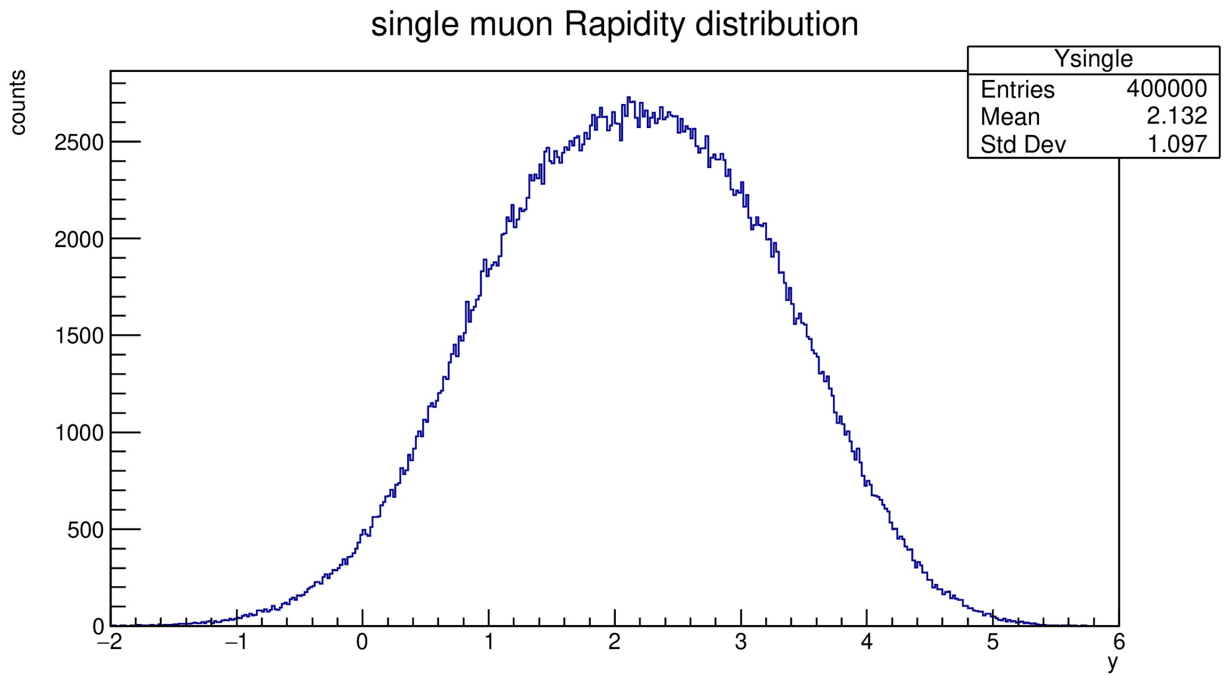

Figure 4.13: The rapidity distribution for each muon

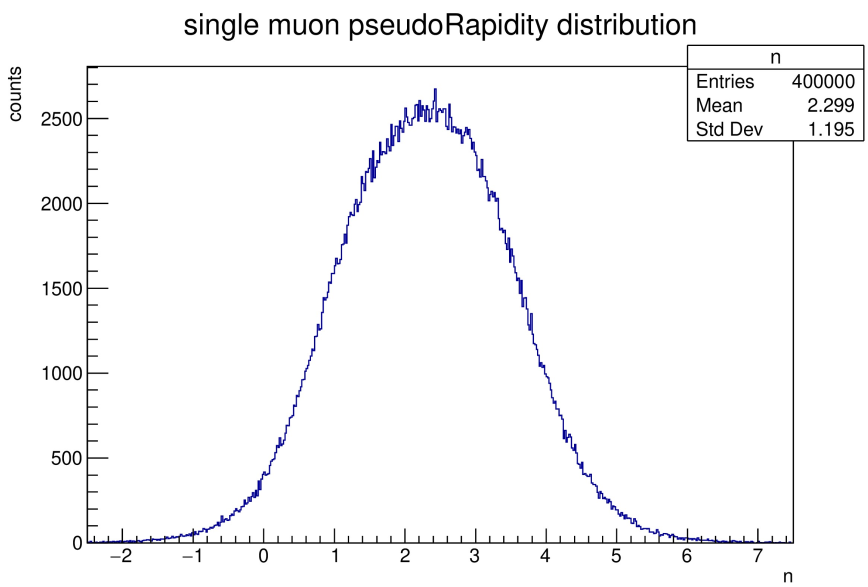

Figure 4.14: The pseudorapidity distribution for each muon

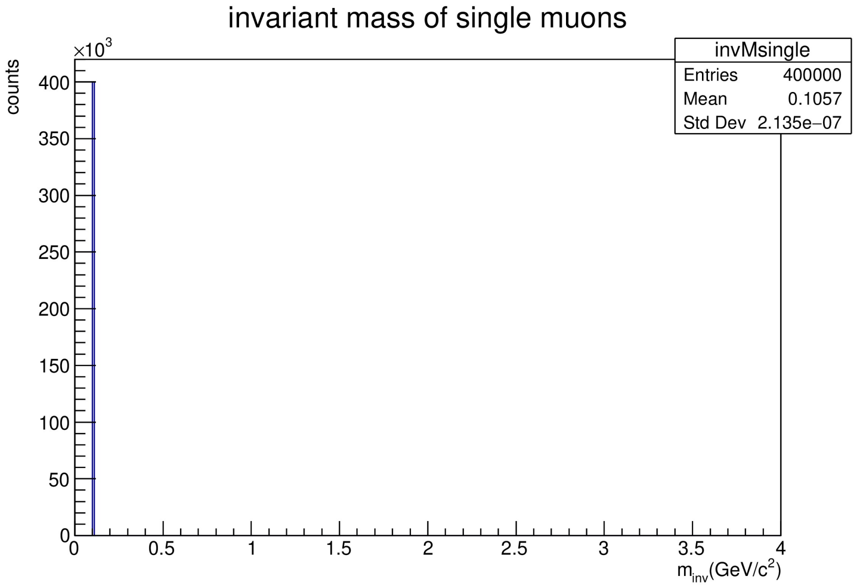

Figure 4.15: The invariant mass distribution for each muon

we see that it peaks only at around 0.2 GeV, since these are real muons and their invariant mass is fixed. Because of the fixed invariant mass of muons, we donot get a continuum in this case.

4.3 Analysis of various kinematic variables of the signal dimuons after passing them through the CBM setup

In this section, we have passed the signal dimuons through the entire CBM setup and reconstructed various kinematic variables related to them.The simulation has been done for thermal dimuons created using only the PLUTO event generator.

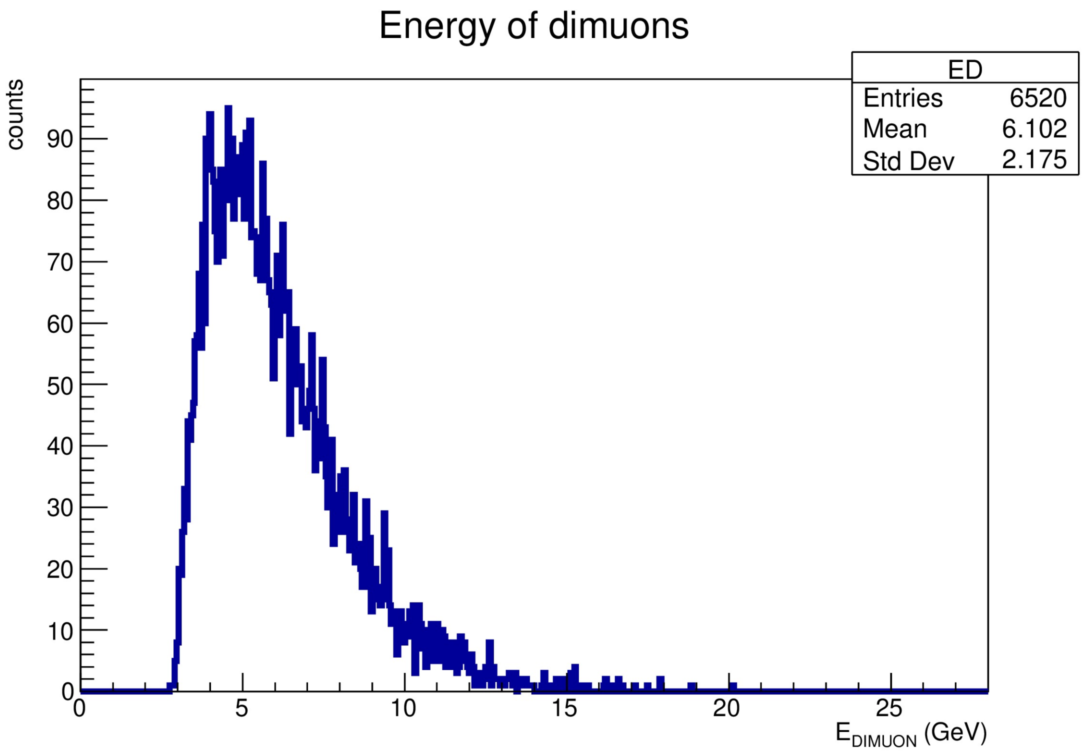

Figure 4.16: The energy distribution of reconstructed dimuons.

In figure 4.16, We can see that very small amount of low energy dimuons reach the final detector in the MUCH setup. The energy distribution of the reconstructed dimuons varies exponentially with increase in energy as should be expected since the initial signal dimuons obey boltzmann statistics.

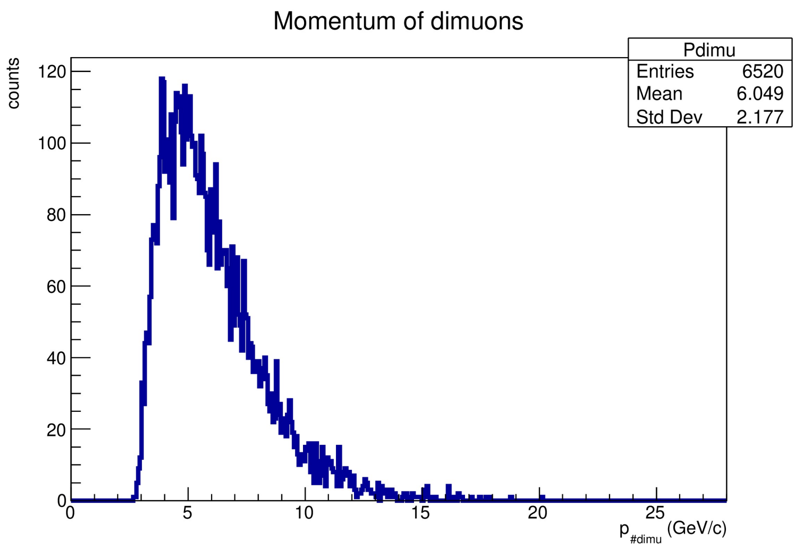

Figure 4.17: The momentum distribution of reconstructed dimuons.

In figure 4.17, We observe that the low momentum muons mostly get absorbed and the momentum distribution decreases exponentially with increase in momentum.

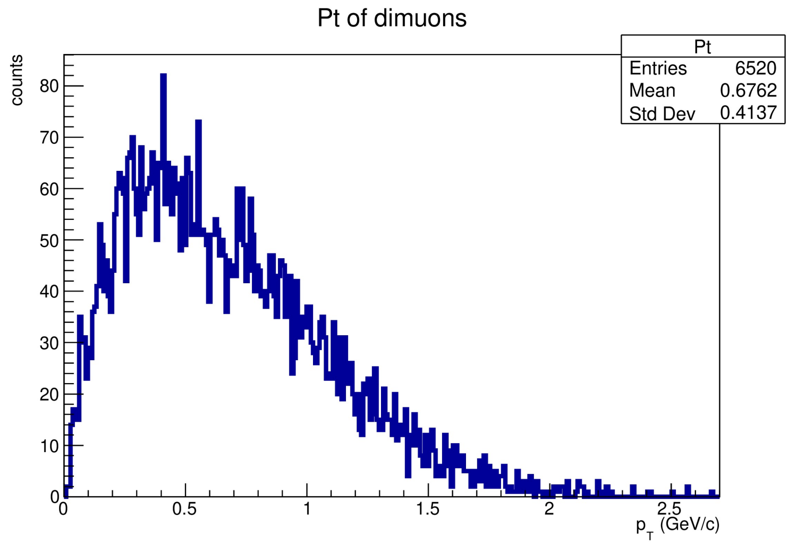

Figure 4.18: The transverse momentum distribution of reconstructed dimuons.

In figure 4.18, we obsereve that the transverse momentum distribution first increases and then decreases exponentially and very small amount of high transverse momentum muons reach the final detector.

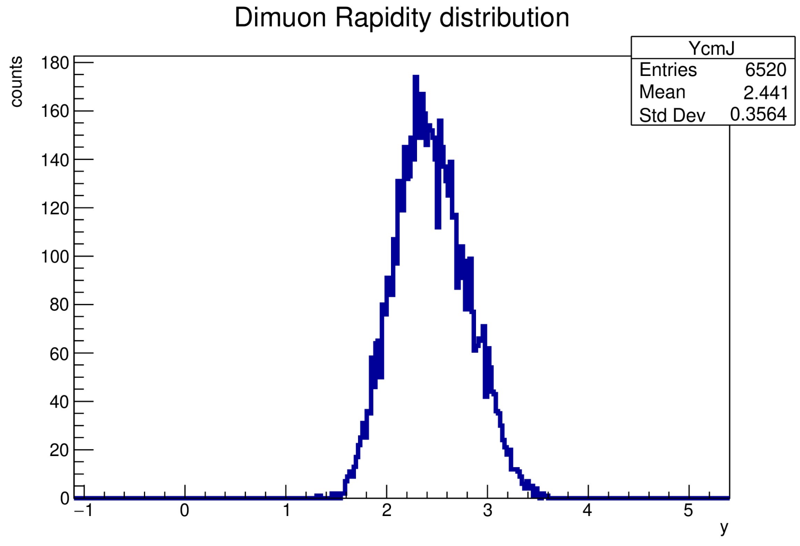

Figure 4.19: The rapidity distribution of reconstructed dimuons.

In figure 4.19, We observe that the low rapidity muons don't reach the final detector and get absorbed.The rapidity distribution is shifted towards the forward direction as it should be , Since the initial events are fixed target collision.

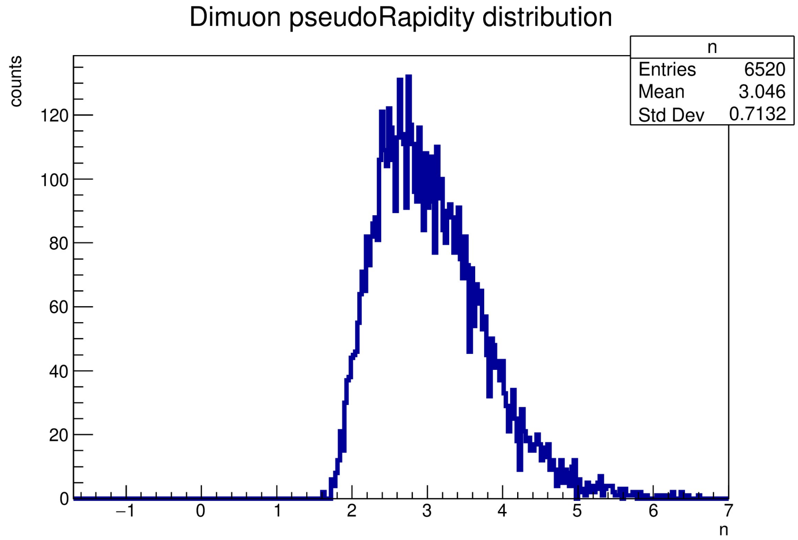

Figure 4.20: The pseudorapidity distribution of reconstructed dimuons.

In figure 4.20, We see that all the muons with low pseudorapidity are absorbed and muons with high value of pseudorapidity are detected in the final detector.

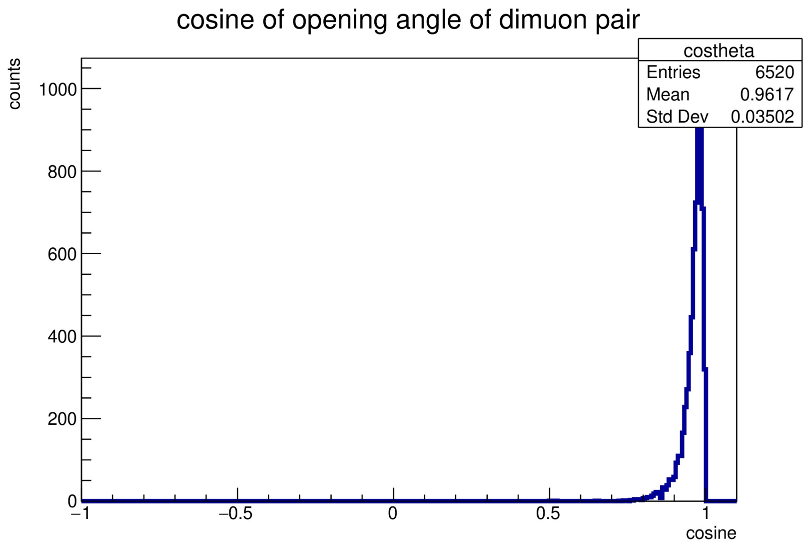

Figure 4.21: The distribution of cosine of the opening angle of reconstructed dimuon pair .

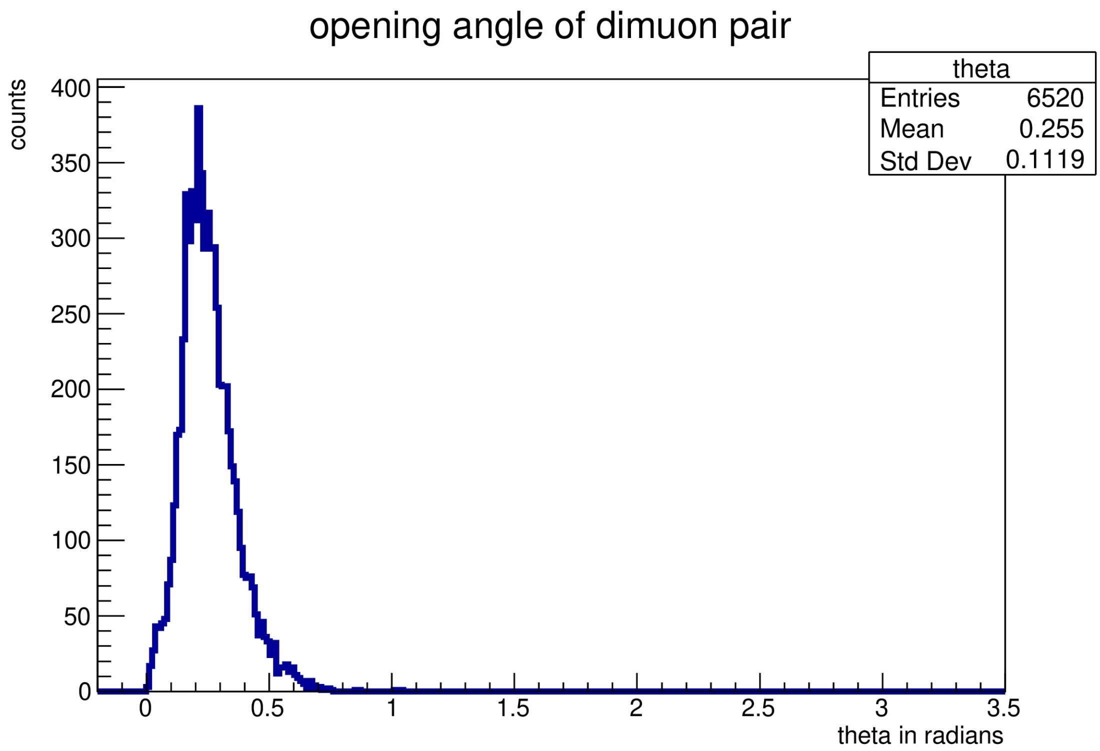

Figure 4.22: The distribution of the opening angle of reconstructed dimuon pair .

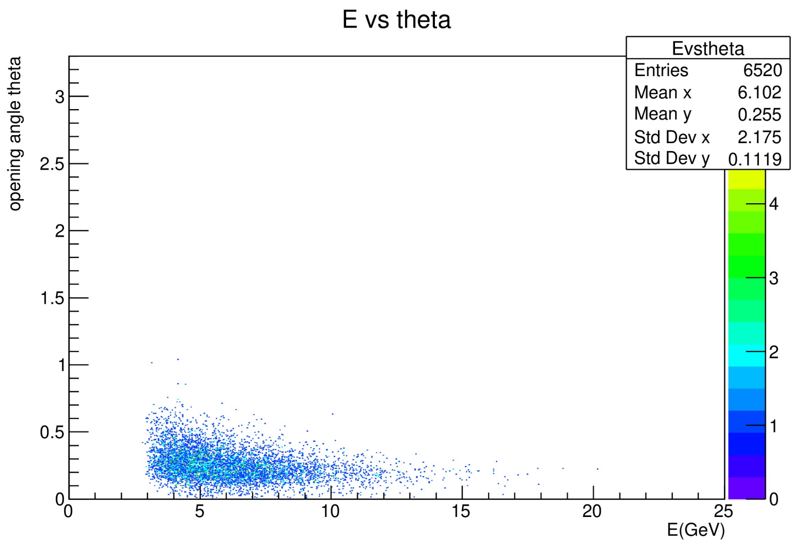

Figure 4.23: The distribution of the opening angle with respect to energy for reconstructed dimuon pair .

From figure 4.23 , We find that the dimuon pairs that have energy less than around 0.3 GeV do not reach the final detector. Very small number of very high energy dimuons reach the final detector because very few extremely high energy dimuons are created. In the intermediate region of energy, the dimuons reach as they are produced enough in number and have sufficient energy to reach the final detector.Hence, dimuons with small opening angles reach the final detector in plentiful.

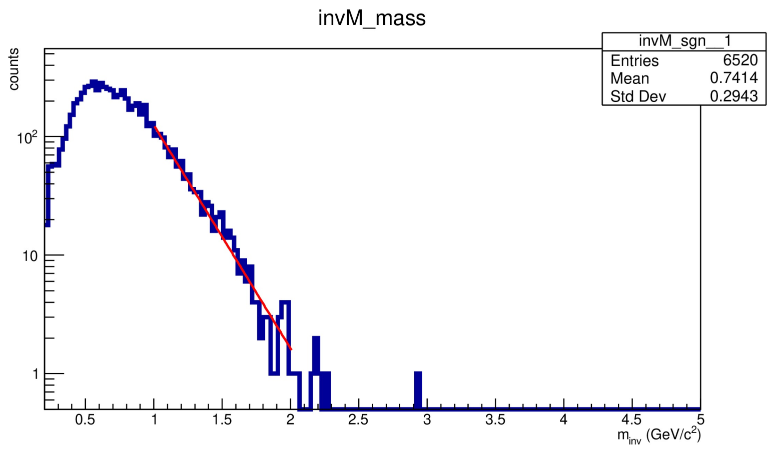

Figure 4.24: Invariant mass distribution of reconstructed thermal dimuons for complete range of transverse momentum.

In figure 4.24, We have plotted the invariant mass distribution of the reconstructed thermal dimuons after passing the thermal dimuons through the entire CBM setup. We have made an exponential fit in the mass range from 1 GeV to 2 GeV and obtained the slope, which is the inverse of the space-time average temperature. Here

α = 9.1601

β = -4.3342

χ^2 = 1.3

Hence the obtained temperature from the invariant mass distribution of the thermal dileptons for complete range of transverse momentum is 230.72±7.17 MeV.

We have also obtained the invariant mass distribution of the reconstructed thermal dimuons for different ranges of transverse momentum p_t spanning from 0 GeV to 2 GeV.

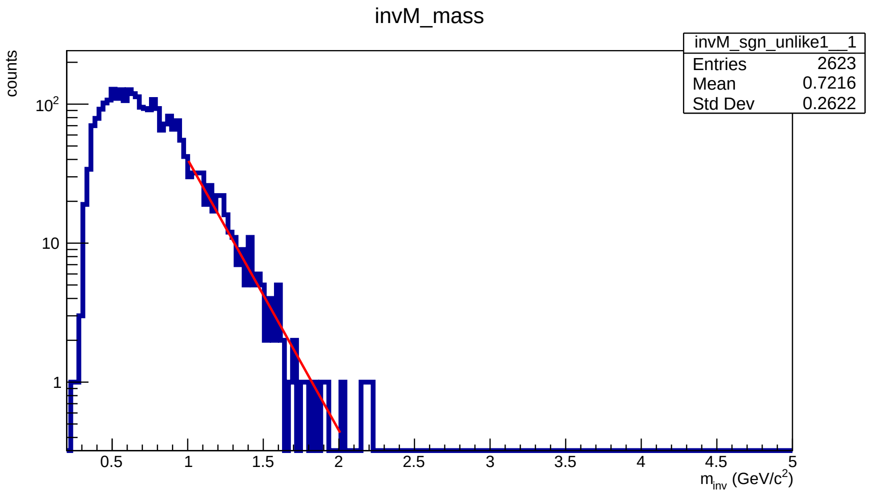

Figure 4.25: Invariant mass distribution of reconstructed thermal dimuons having transverse momentum between 0.0 GeV/C to 0.5 GeV/C

In figure 4.25, We have obtained the invariant mass distribution of the reconstructed dimuons pairs for the p_t range from 0.0 GeV/C to 0.5 GeV/C and fitted it exponentially between the mass range from 1 GeV to 2 GeV. Here

α = 8.1752

β = -4.4873

χ^2 = 1.3

The inverse of the slope gives the effective space-time averaged temperature of the QGP and the value of the temperature obtained is 222.84$\pm$3.42MeV.

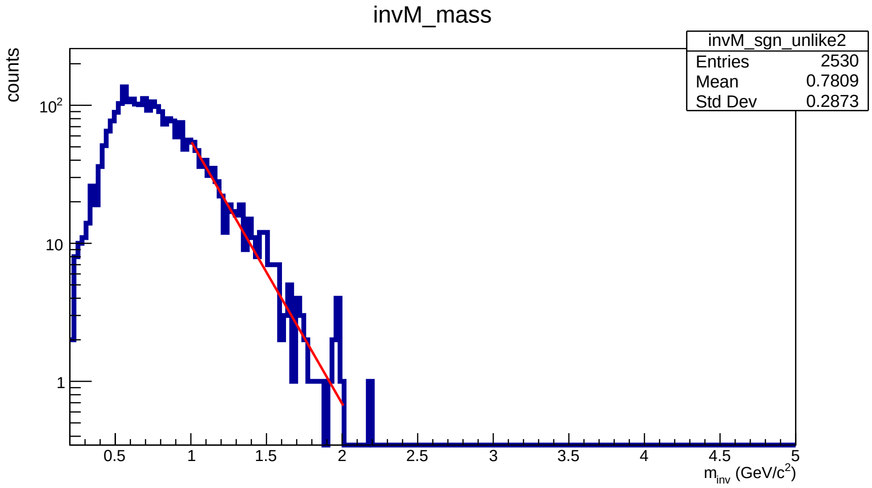

Figure 4.26: Invariant mass distribution of reconstructed thermal dimuons having transverse momentum between 0.5 GeV/C to 1 GeV/C

In figure 4.26, We have obtained the invariant mass distribution of the reconstructed dimuonn pairs for the p_t range from 0.5 GeV/C to 1 GeV/C and fitted it exponentially between the mass range from 1 GeV to 2 GeV. Here

α = 8.3899

β = -4.3798

χ^2 = 1.3

The inverse of the slope gives the effective space-time averaged temperature of the QGP and the value of the temperature obtained is 228.31$\pm$4.28MeV.

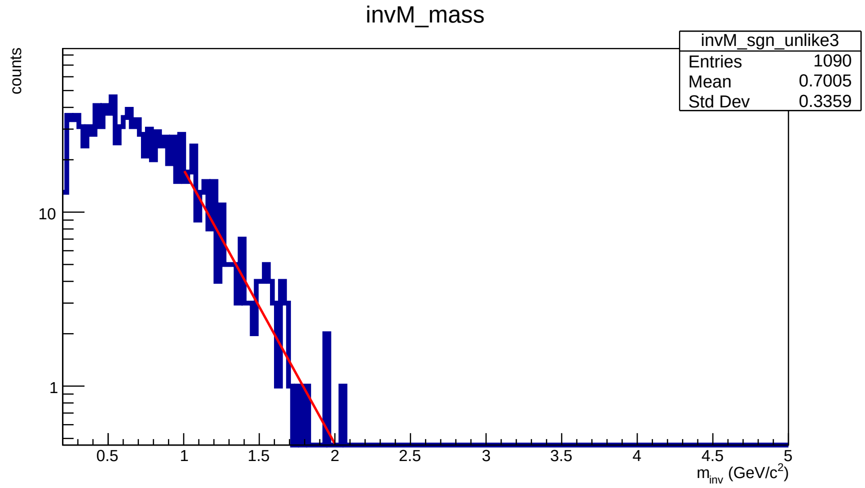

Figure 4.27: Invariant mass distribution of reconstructed thermal dimuons having transverse momentum between 1 GeV/C to 1.5 GeV/C

In figure 4.27, We have obtained the invariant mass distribution of the reconstructed dimuonn pairs for the p_t range from 1 GeV/C to 1.5 GeV/C and fitted it exponentially between the mass range from 1 GeV to 2 GeV. Here

α = 6.4915

β = -3.6280

χ^2 = 1.3

The inverse of the slope gives the effective space-time averaged temperature of the QGP and the value of the temperature obtained is 275.63$\pm$2.2MeV.

Table 4.1: Tabulated summary of PLUTO analysis

Type of signal	p_t **Range(In GeV/C)**	α	β	**Temperature(In MeV)**
Pure PLUTO	All p_t	10.6400	-4.4568	224.37 $\pm$3.36
Reconstructed PLUTO	All p_t	9.1601	-4.3342	230.72 $\pm$7.17
Reconstructed PLUTO	0.0 to 0.5	8.1752	-4.4873	222.84 $\pm$3.42
Reconstructed PLUTO	0.5 to 1.0	8.3899	-4.3798	228.31 $\pm$4.28
Reconstructed PLUTO	1.0 to 1.5	6.4915	-3.6280	275.63 $\pm$2.20

4.4 Analysis of the background particles

Now in a real heavy-ion collision, there will be initial production of huge amount of background particles. hadrons and their resonances will be produced. The MUCH detector is designed to construct the invariant mass distribution of all the muons that reaches the final detector. Now muons can come from decay of low mass hadronic resonance states like ρ, ω and ϕ. They may also arise from the decay of high mass states like j/ψ and ψ'. Muons can also reach the final detector of the MUCH detector setup from weak meson decay. A large part of the physical background comes from Drell-Yan process and semileptonic decay of heavy flavor mesons like D, $\overline{D}$ etc. Dalitz decay also contributes to the muon spectra. Decay of kaons and pions also contributes to the muon invariant mass spectra. So for a more realistic analysis of heavy ion collisions and in particular, to understand the efficiency of the MUCH detector with respect to determination of thermal dimuons, we need to include not only the signal thermal dimuons from the PLUTO generator, but we also need to input all the necessary background particles that may arise in the heavy ion collision. One of the way to do so is to create the background particles using an event generator called UrQMD which stands for ultra-relativistic quantum molecular dynamics. UrQMD uses various models from perturbative QCD , Lattice QCD and various transport models or hydrodynamic models to calculate the production cross-section as well as interaction cross-section of various particles that may arise in a heavy ion collision. It takes help of various effective models to produce particles at different energy ranges. UrQMD can be used to effectively generate background particles from collision energies ranging from 2 A GeV to 200 A GeV. So, For our simulation purposes, we use UrQMD to generate background particles and pass them through the CBM setup. Finally the inavariant mass distribution of the background particles is obtained both for the entire range of transverse momentum p_t as well as for different ranges of p_t .

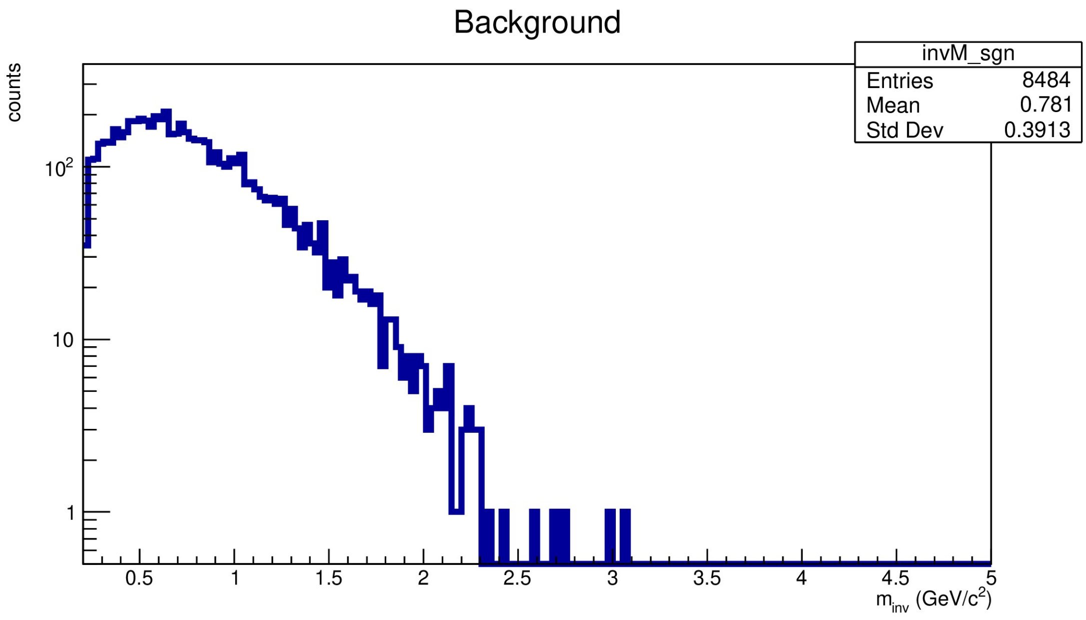

Figure 4.28: Invariant mass distribution of the reconstructed background for the entire p_t range.

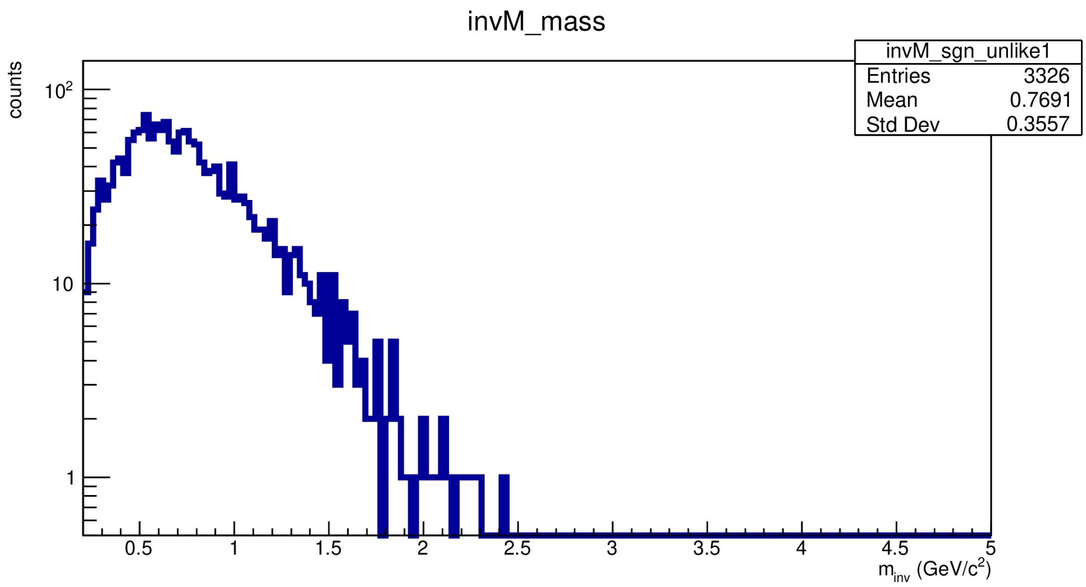

Figure 4.29: Invariant mass distribution of the reconstructed background for the p_t range from 0.0 GeV/C to 0.5 GeV/C.

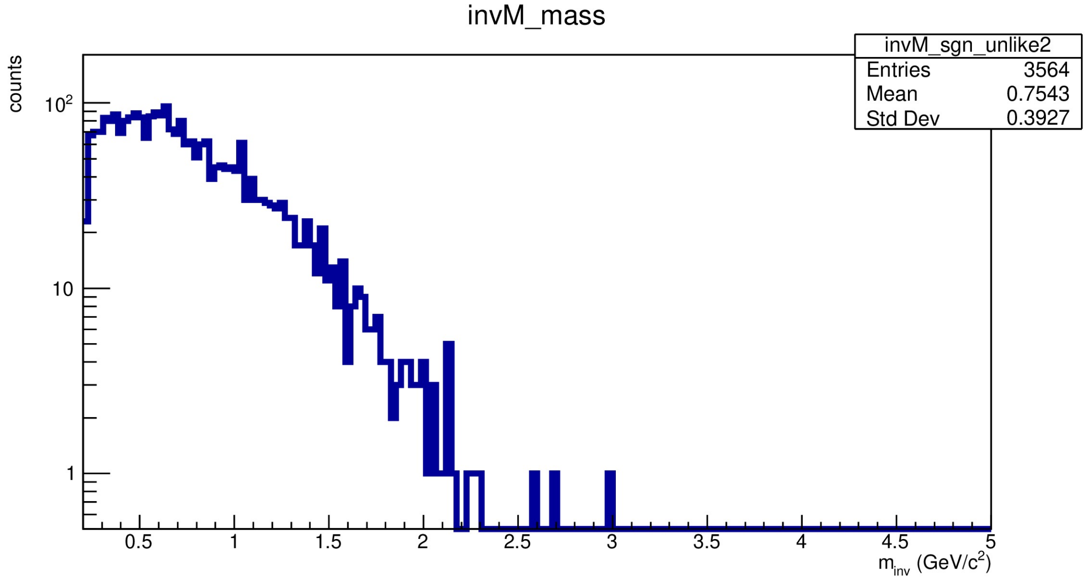

Figure 4.30: Invariant mass distribution of the reconstructed background for the p_t range from 0.5 GeV/C to 1 GeV/C.

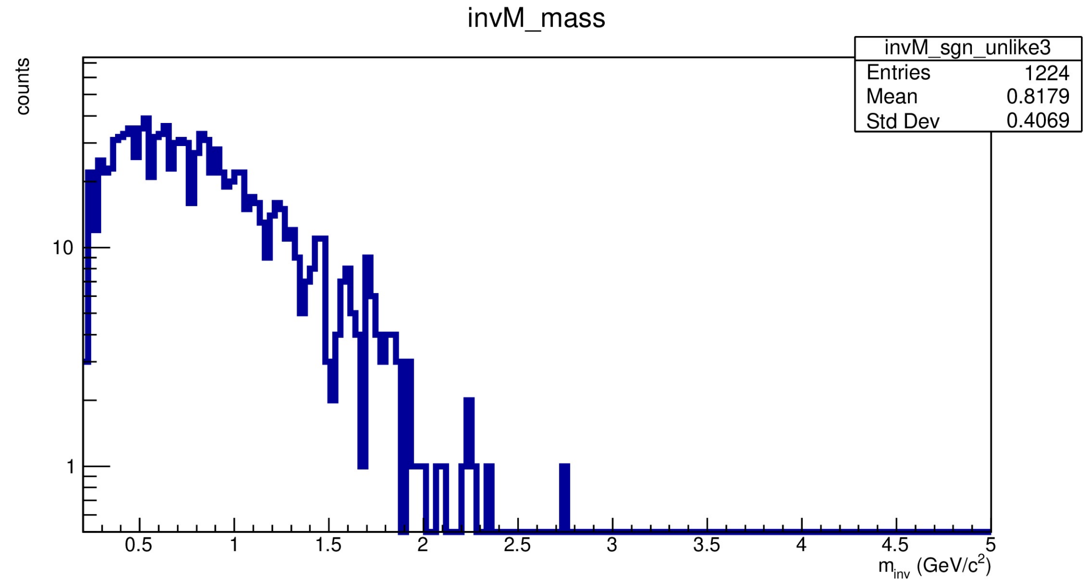

Figure 4.31: Invariant mass distribution of the reconstructed background for the p_t range from 1 GeV/C to 1.5 GeV/C.

4.5 Analysis of the signal and background combined together

To simulate realistic heavy ion collisions, we need to send both the signal thermal dimuons as well as the generated background together and then reconstruct the invariant mass spectra of the total muon candidates detected at the last detector of the MUCH detector setup. In this section we have generated 200k pairs of thermal dimuons using PLUTO event generator and 200k events of Au-Au collision in the minimum bias condition to produce the background particles using UrQMD event generator. The entire signal and background is sent through the CBM experiment setup.

First, In figure 4.32, We have obtained the invariant mass spectra of the combined signal and background for the complete range of transverse momentum p_t.

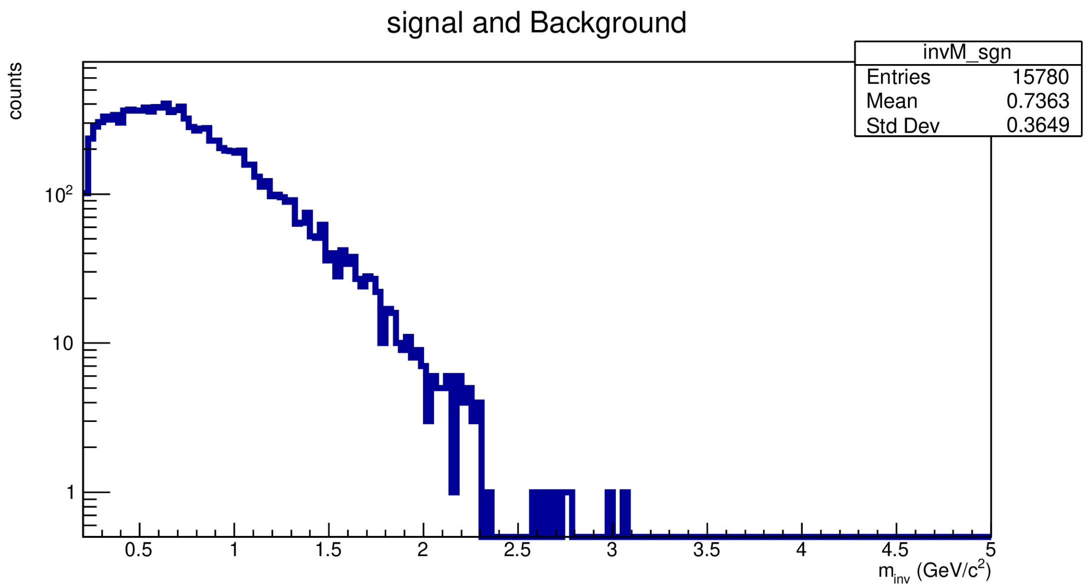

Figure 4.32: Invariant mass distribution of the reconstructed combined signal and background for the complete p_t range

Next we have obtained the invariant mass spectra of the reconstructed combined signal and background for different ranges of transverse momentum p_t.

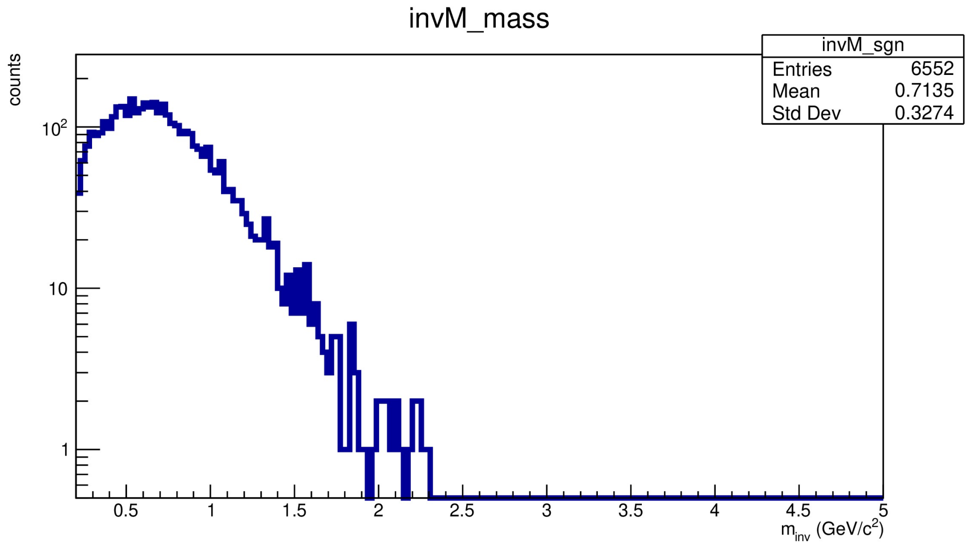

Figure 4.33: Invariant mass distribution of the reconstructed combined signal and background for the p_t range from 0.0 GeV/C to 0.5 GeV/C.

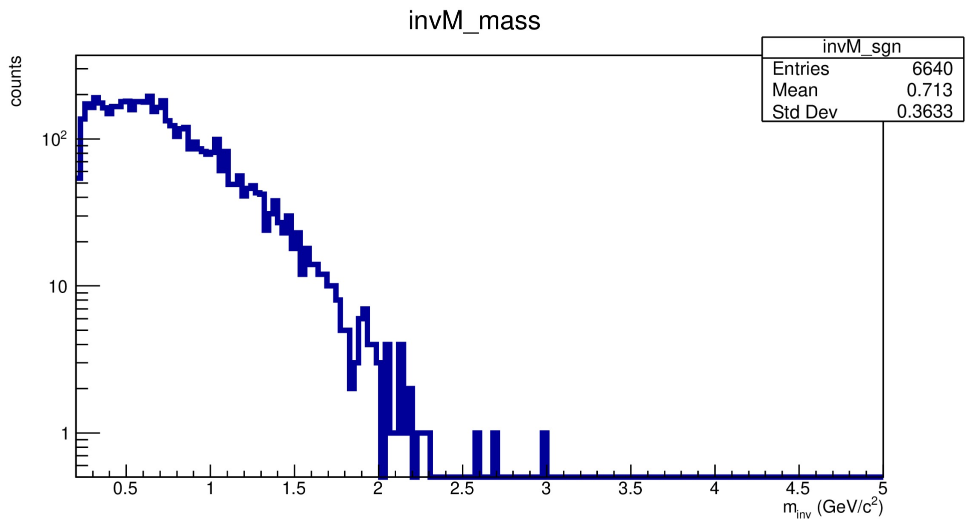

Figure 4.34: Invariant mass distribution of the reconstructed combined signal and background for the p_t range from 0.5 GeV/C to 1 GeV/C.

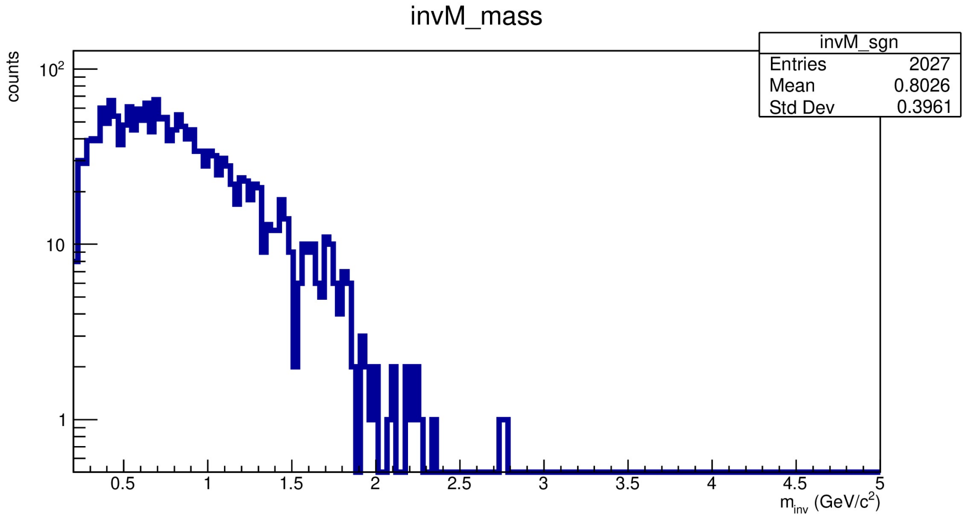

Figure 4.35: Invariant mass distribution of the reconstructed combined signal and background for the p_t range from 1 GeV/C to 1.5 GeV/C.

We have obtained the invariant mass distribution of the combined signal and background for the different p_t range.

4.6 Analysis of the reconstructed signal after removing the background from complete spectra.

In realistic heavy ion collisions, we will get complete spectra including the signal and background. To extract essential information related to experimentally important signal, we would need to remove the unnecessary background from the complete spectra.

In this simulation work, we have subtracted the reconstructed background created using UrQMD from the total reconstructed spectra created using both PLUTO as well as UrQMD. We have obtained the total reconstructed signal obtained after subtraction of the background. This signal should in principle just be the thermal dimuons. So we have obtained the invariant mass spectra of the subtracted signal for the entire range of transverse momentum p_t as well as for different ranges of p_t. We have fitted the invariant mass spectra in each case with the exponential function between the mass range from 1 GeV to 2 GeV and obtained the slope , which is the inverse of the space-time average temperature of the QGP formed in the collision events.

First, In figure 4.36, We have obtained the invariant mass spectra of the subtracted signal for the entire p_t range and then exponentially fitted the obtained invariant mass in the mass range from 1 GeV to 2 GeV to obtain the inverse temperature.

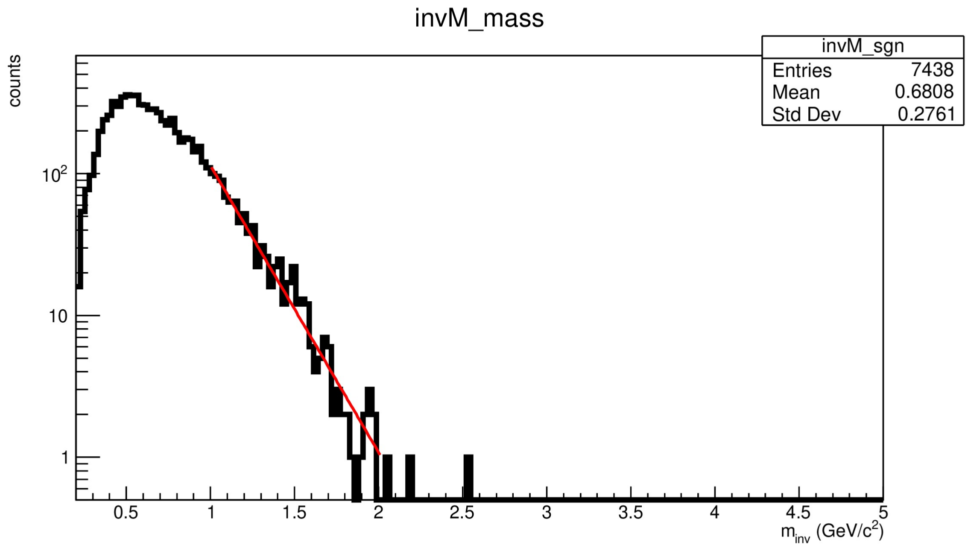

Figure 4.36: Invariant mass distribution of the reconstructed signal obtained after subtracting the background from the entire combined signal and background for entire p_t range

We have obtained the temperature from the exponential fit in the mass range from 1 GeV to 2 GeV for the invariant mass distribution of the subtracted signal for the entire p_t range . Here

α = 8.9257

β = -4.6537

χ^2 = 1.3

and the temperature obtained is 214.88 ± 5.83 MeV.

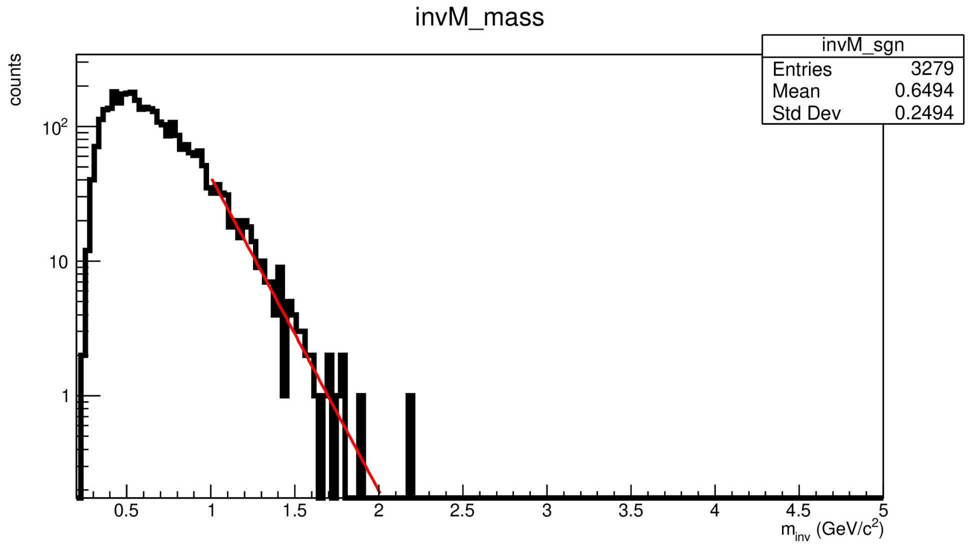

Figure 4.37: Invariant mass distribution of the reconstructed signal obtained after subtracting the background from the entire combined signal and background for p_t range from 0.0 GeV/C to 0.5 GeV/C

From figure 4.37, we obtain the fitting parameter values as

α = 9.2107

β = -4.6869

χ^2 = 1.3

As can be inferred from figure 4.37, The obtained temperature from the exponential fit in the mass range from 1 GeV to 2 GeV for the invariant mass distribution of the subtracted signal for the p_t range from 0.0 GeV/C to 0.5 GeV/C is 213.36 ± 2.65 MeV.

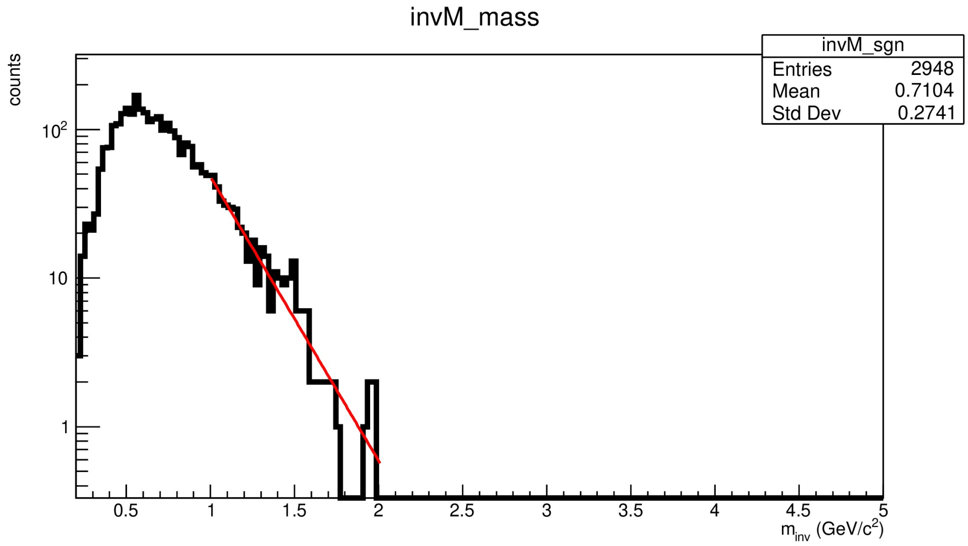

Figure 4.38: Invariant mass distribution of the reconstructed signal obtained after subtracting the background from the entire combined signal and background for p_t range from 0.5 GeV/C to 1 GeV/C

From figure 4.38, The values of the fitting parameters are

α = 9.3768

β = -4.4008

χ^2 = 1.3

In figure 4.38, The obtained temperature from the exponential fit in the mass range from 1 GeV to 2 GeV for the invariant mass distribution of the subtracted signal for the p_t range from 0.5 GeV/C to 1 GeV/C is 227.23 ± 3.49 MeV.

Table 4.2: Tabulated summary of analysis of signal obtained after background subtraction

Type of signal	p_t **Range(In GeV/C)**	α	β	**Temperature(In MeV)**
After background subtraction	All p_t	8.9257	-4.6537	214.88 $\pm$5.83
After background subtraction	0.0 to 0.5	9.2107	-4.6869	213.36 $\pm$2.65
After background subtraction	0.5 to 1.0	9.3768	-4.4008	227.23 $\pm$3.49

4.7 Conclusion and Future Scope of this Work.

Table 4.3: Tabulated summary of analysis for pure PLUTO, Reconstructed PLUTO as well as for signal obtained after background subtraction.

Type of signal	p_t **Range(In GeV/C)**	α	β	**Temperature(In MeV)**
Pure PLUTO	All p_t	10.6400	-4.4568	224.37 ±3.36
Reconstructed PLUTO	All p_t	9.1601	-4.3342	230.72 ±7.17
Reconstructed PLUTO	0.0 to 0.5	8.1752	-4.4873	222.84 ±3.42
Reconstructed PLUTO	0.5 to 1.0	8.3899	-4.3798	228.31 ±4.28
Reconstructed PLUTO	1.0 to 1.5	6.4915	-3.6280	275.63 ±2.20
After background subtraction	All p_t	8.9257	-4.6537	214.88 ±5.83
After background subtraction	0.0 to 0.5	9.2107	-4.6869	213.36 ±2.65
After background subtraction	0.5 to 1.0	9.3768	-4.4008	227.23 ±3.49

The primary conclusion that can be drawn from the above simulation studies is that the MUCH detector setup in the CBM experiment can be well optimized to detect the thermal dileptons and hence be used to obtain the space-time average temperature of the QGP state created in heavy ion collisions. The CBM experiment will start at around the year 2025. So, these simulations can give us some idea what kind of thermal signatures can we expect to be detected by the detector setup once the experiment finally turns on and real data is collected. Ofcourse various invariant mass techniques will be used to remove the unwanted backgrounds. The CBM experiment will produce high baryon density quark-gluon plasma which has never been created by any other accelerator facility in the world. So, there are various theoretical models right now that are being developed to understand that at what p_t range can we expect QGP signature particularly at the low energies. These simulations can be used to get some insight into developing such models. Ofcourse more analysis needs to be done. It has been observed that for 8 A GeV collisions, the number of high p_t thermal dimuons that reach the final detector is very small. However , if we increase the colliding energies,more high p_t thermal dimuons will reach the final detector. A drawback of doing this is that the baryon density of the created QGP will decrease as the colliding nucleons will pass through each other faster instead of stopping to interact as the overlap time of the colliding nucleons will decrease. A way around this problem is to use extremely huge amounts of events. In our case we used 200k thermal dimuon pairs, and obtained thermal dimuons in the final detector of the order of around 6000. A better simulation study would be to use thermal dimuons of the order of 40 lakh which would give atleast 1 lakh thermal dimuons on the final detector.This would demand huge amount of computation power.This would help us to get better estimates on the temperature measurement capabilities of the CBM experiment.The present version of the MUCH geometry does not include some electronic circuit boards, as they will be included into MUCH geometry in future, the simulation will have to be repeated to further optimize the complete detector system. We have done the simulation for SIS100-B setup of the MUCH geometry which is suitable for analysis in the energy range between 8 A GeV to 10 GeV. For collision events with higher energy, more background particles will reach the final detector layer of SIS100-B setup, so, We need to use detector geometries with more hadron absorber layers. So, We will need to use MUCH geometry versions like SIS100-C for energy upto 29 A GeV and so on.However, the basic simulation procedure will be similiar to the one done in this work.

Bibliography

[1] Ramona vogt- Ultrarelativistic heavy-ion collisions (2007, Elsevier) *ISBN.* 0444521968, 9780444521965, 9780080525365.

[2] Cheuk-Yin Wong *Introduction to High-Energy Heavy-Ion Collisions ISBN.* 9810202636, 9789810202637

[3] Lecture Notes in Physics 814,Springer *The CBM Physics Book ISBN.* 9783642132933, 3642132936

[4] Phenomenology-of-Ultra-relativistic-Heavy-ion-Collisions, Wojciech Florkowski, world scientific. *ISBN.* 9814280682, 9789814280686

[5] Technical design report-MUCH *by The CBM collaboration*

[6] GEANT user guide version 3.15

[7] ROOT user guide

[8] Design of the Pluto Event Generator by I. Froehlich, T. Galatyuk, R. Holzmann, J. Markert, B. Ramstein, P. Salabura, J. Stroth *DOI.* 10.1088/1742-6596/219/3/032039

[9] CHARMONIUM PRODUCTION AND DETECTION IN HIGH ENERGY NUCLEAR COLLISIONS AT FAIR, Phd Thesis, Partha Pratim Bhaduri, VECC, Kolkata

[10] Thermal Dileptons as Fireball Thermometer and Chronometer, Ralf Rapp, Hendrik van Hees arXiv:1411.4612 [hep-ph]